

1 Supporting Information for:

2 **Photooxidants from Brown Carbon and Other Chromophores in**  
3 **Illuminated Particle Extracts**

4 Richie Kaur<sup>1</sup>, Jacqueline R. Labins<sup>1</sup>, Scarlett S. Helbock<sup>1</sup>, Wenqing Jiang<sup>2</sup>, Keith J.  
5 Bein<sup>3</sup>, Qi Zhang<sup>2</sup>, Cort Anastasio<sup>1,\*</sup>

6 <sup>1</sup>Department of Land, Air and Water Resources, University of California-Davis, One Shields Avenue,  
7 Davis, CA 95616-8627, USA

8 <sup>2</sup>Department of Environmental Toxicology, University of California-Davis, One Shields Avenue, Davis,  
9 CA 95616-8627, USA

10 <sup>3</sup>Center for Health and the Environment, University of California-Davis, One Shields Avenue, Davis, CA  
11 95616-8627, USA

12  
13 Correspondence to: C. Anastasio ([canastasio@ucdavis.edu](mailto:canastasio@ucdavis.edu))

14  
15 This supporting information contains: 19 Tables, 13 Figures and 5 Sections

16  
17 Submitted to Atmospheric Chemistry and Physics, 2 December 2018

18 **Table S1.** Sample collection details and light absorption of particle extracts

Sample ID	Collection Dates	Collection Times <sup>d</sup>	Average hourly PM <sub>2.5</sub> concentration <sup>e</sup> (μg/m <sup>3</sup> -air)	$\alpha_{300}$ <sup>f</sup> (cm <sup>-1</sup> )	Average Mass of PM extracted <sup>g</sup>	$R_{\text{abs}}$ (300-450nm) <sup>h</sup> (10 <sup>-6</sup> mol-photons L <sup>-1</sup> s <sup>-1</sup> )	$f_{\text{Rabs IN}}$ <sup>i</sup>	MAC <sub>DOC</sub> (300 nm) <sup>j</sup> (10 <sup>4</sup> cm <sup>2</sup> g <sup>-1</sup> -C)	AAE <sup>k</sup>	Light Screening Factor <sup>l</sup>
Particle Extracts										
PME1 <sup>*a</sup>	01/06/16 - 01/08/16	17:30 - 07:30 (N)	5.8 (2.1)	0.077	105 (16)	1.7	0.00080	2.6	6.8	0.98
PME2 <sup>*a</sup>	12/18/15 - 12/20/15	17:30 - 07:30 (N)	15 (10)	0.100	269 (30)	1.8	0.0059	2.0	7.2	0.97
PME3 <sup>b</sup>	01/26/16 - 01/29/16	10:20 - 09:45 (C)	16 (11)	0.272	328 (19)	4.2	0.0076	1.3	7.9	0.93
PME4 <sup>b</sup>	12/16/15 - 12/18/15	17:30 - 07:30 (N)	20 (8)	0.567	350 (14)	12	0.0031	2.6	6.4	0.85
PME5 <sup>b</sup>	01/10/16 - 01/12/16	17:30 - 07:30 (N)	5.9 (3.4)	0.317	132 (11)	7.4	0.00080	2.6	6.2	0.91
PME6 <sup>b</sup>	01/23/16 - 01/26/16	17:30 - 07:30 (N)	6.8 (2.9)	0.584	174 (14)	13	0.00058	3.0	6.9	0.84
PME3D0.5 <sup>c</sup>				0.556	323 (21)	8.8			7.7	0.87
PME3D1.3 <sup>c</sup>				0.199	315 (23)	3.2	0.0071	1.3	7.6	0.95
PME3D2.5 <sup>*a</sup>				0.103	331 (15)	1.7	0.0092	1.3	7.6	0.97
PME3D10 <sup>c</sup>				0.0263	347	0.42	0.0062	1.3	7.6	0.99
Averages (±σ)										
“Standard” (PME3-6)				0.44 (0.16)		9.1 (4.1)	0.0030 (0.0033)	2.4 (0.7)	6.8 (0.7)	
“Dilute” (PME1*-2*,3D2.5*)				0.093 (0.014)		1.7 (0.1)	0.0053 (0.0042)	2.0 (0.6)	7.2 (0.4)	
Davis Fog <sup>m</sup>				0.094 (0.047)		1.8 (0.9)	0.0082 (0.0031)	1.3 (0.1)	6.6 (0.5)	
Test statistic <sup>n</sup>				<b>0.021</b>		<b>0.035</b>	0.061	<b>0.013</b>	0.56	
Field Blanks										
FB1 <sup>a</sup>	12/18/15	09:38 - 09:40		0.0025	17.8 (7.6)	0.024				
FB2 <sup>b</sup>	01/20/16	10:08 - 10:10		0.0037	24.9 (9.1)	0.022				

19 <sup>a</sup> Samples extracted in 2.5 mL/filter square and referred to as the “dilute” extracts in the main text.

20 <sup>b</sup> PME3-6 were extracted as 1 mL/filter square and are referred to as “standard” extracts in the main text.

21 <sup>c</sup> PME3D0.5, PME3D1.3 and PME3D10 are extracts of sample PME3 using varying extraction volumes per filter square, namely 0.5 , 1.3 and 10  
22 mL, respectively.

23 <sup>d</sup> N = Night-time samples, collected from 17:30 on one day until 07:30 AM the next day; this was done for consecutive days on the same filter. C  
24 = Continuous collection for the indicated number of days.

25 <sup>e</sup> Average (± 1σ) hourly PM<sub>2.5</sub> concentration for each sampling period measured at the UC Davis sampling site by the California Air Resources  
26 Board as reported on the iADAM online database (California Air Resources Board, 2018).

27 <sup>f</sup> Base-10 absorbance of the extract (in cm<sup>-1</sup>) at 300 nm.

28 <sup>g</sup> Average (± 1σ) mass of PM extracted from each filter square for a given sample.

29 <sup>h</sup> Rate of sunlight absorption by each extract in the 300 – 450 nm wavelength range (Eq. (2), main text).

30 <sup>i</sup> Fraction of calculated sunlight absorption due to inorganic nitrogen (nitrite and nitrate) in each sample. Equations are in Kaur and Anastasio  
31 (2017).

32 <sup>j</sup> Mass absorption coefficient of dissolved organic species at 300 nm for each sample (Eq. (3), main text) in units of 10<sup>4</sup> cm<sup>-2</sup> g<sup>-1</sup>-C.<sup>1</sup>

33 <sup>k</sup> Absorption Angstrom Exponent (AAE), calculated as the negative of the slope of a linear regression of the extract absorbance data between 300  
34 and 450 nm versus the log of the wavelength:  $\log(\text{Abs}_\lambda) = \log(\text{Abs}_{300}) - \text{AAE} \times \log(\lambda)$ , where  $\lambda$  is the wavelength and  $\text{Abs}_\lambda$  and  $\text{Abs}_{300}$  are the  
35 absorbance values at  $\lambda$  and 300 nm, respectively.

36 <sup>1</sup> Light-absorption-weighted internal screening factor, calculated as  $S_{\lambda} = \frac{\Sigma[(1-10^{-\alpha_{\lambda}l}) \times I'_{\lambda}]}{\Sigma[(2.303 \times \alpha_{\lambda}l) \times I'_{\lambda}]}$ . In this equation,  $\alpha_{\lambda}$  is the pathlength-normalized

37 absorbance of the extract at each wavelength, summed for the wavelength range in which light absorption by the extracts was the highest (280-  
38 350 nm);  $l$  is the pathlength of the quartz tube used for illuminating the extracts (0.4 cm);  $I'_{\lambda}$  is the actinic flux (mol-photons L<sup>-1</sup> s<sup>-1</sup>) of the  
39 illumination system, calculated using the photon count of the illumination system measured using a TIDAS Photo Diode Array Spectrometer  
40 and the measured pseudo-first-order rate constant for loss of our chemical actinometer, 2-nitrobenzaldehyde. The numerator represents the  
41 actual rate of light absorption by all chromophores in the extract while the denominator is the estimated rate of light absorption in the extract  
42 assuming it is low light-absorbing. A value of 1.0 indicates no light screening (Smith et al., 2014; Rehorek and Seidel, 1989).

43 <sup>m</sup> Average values previously measured in Davis fog samples (n = 4) (Kaur and Anastasio, 2017).

44 <sup>n</sup> Test statistic for comparison of standard PME and Davis fog averages:  $p$ -value for a two-tailed  $t$ -test for samples of unequal variance. Values  
45 below 0.05 are in bold.

46 **Table S2.** Chemical characteristics of particle extracts

Sample ID	DOC μM-C	[NO <sub>2</sub> ] μM	[NO <sub>3</sub> ] μM	[SO <sub>4</sub> <sup>2-</sup> ] μM	[Cl] μM	[HCOO <sup>-</sup> ] μM	[NH <sub>4</sub> <sup>+</sup> ] μM	[Na <sup>+</sup> ] μM	[K <sup>+</sup> ] μM	[Ca <sup>2+</sup> ] μM	[Mg <sup>2+</sup> ] μM
Particle Extracts											
PME1 <sup>*a</sup>	562	0.29	113	12.5	15.7	2.1	55.3	82.3	29.9	2.5	0.0
PME2 <sup>*a</sup>	900	2.8	884	31.3	19.8	4.1	751	78.9	43.0	8.3	2.3
PME3 <sup>b</sup>	3610	10.2	2520	302	66.3	13.0	2580	343	171	22.1	3.3
PME4 <sup>b</sup>	4090	8.3	3290	91.1	69.6	21.4	2010	317	197	44.1	11.3
PME5 <sup>b</sup>	2350	3.8	375	22.9	36.7	10.9	287	287	76.7	9.8	2.2
PME6 <sup>b</sup>	3720	5.4	432	65.6	77.7	4.9	276	362	97.2	13.0	7.4
PME3D0.5 <sup>c</sup>	7132	18	4820	533	127	27	5052	681	342	53	6.4
PME3D1.3	2760	6.4	1830	216	48.2	10.5	1600	233	105	20.0	1.6
PME3D2.5 <sup>a</sup>	1400	4.1	1250	195	27.3	5.1	816	118	42.6	4.7	1.3
PME3D10	356	1.2	183	28.1	6.9	1.0	177	24.3	11.9	0.0	0.0
Averages (±σ)											
“Standard” (PME3-6)	3440 (760)	6.9 (2.9)	1650 (1480)	120 (124)	62.6 (17.9)	12.5 (6.8)	1290 (1190)	327 (33)	136 (58)	22.2 (15.5)	6.1 (4.1)
“Dilute” (PME1*- 2*,3D2.5*)	953 (419)	2.4 (1.9)	749 (580)	80 (101)	20.9 (5.9)	3.8 (1.5)	541 (420)	93.2 (21.9)	38.5 (7.4)	5.2 (2.9)	1.2 (1.1)
Davis Fog	1240 (560)	3.4 (6.1)	1080 (630)	120 (84)	22.9 (13.0)	5.1 (2.6)	1070 (550)	- <sup>d</sup>	3.5 (1.9)	4.2 (1.1)	1.4 (0.4)
Test statistic <sup>e</sup>	<b>0.0042</b>	0.35	0.51	0.98	<b>0.013</b>	0.11	0.75	-	<b>0.019</b>	0.10	0.11
Field Blanks											
FB1 <sup>a</sup>	78.9	0	4.5	0.8	9.0	1.1	3.1	63.8	8.3	1.4	0.0
FB2 <sup>b</sup>	244	0	1.1	0.4	6.1	9.0	12.3	143.5	10.9	3.4	0.0
MQ	< DL	< DL	< DL	< DL	< DL	< DL	< DL	1.8	< DL	< DL	< DL

47 <sup>a</sup> Samples extracted in 2.5 mL/filter square and referred to as the “dilute” extracts in the main text.48 <sup>b</sup> Samples extracted in 1mL/filter square and are referred to as “standard” extracts in the main text.49 <sup>c</sup> DOC and IC values for sample PME3D0.5 were not measured due to a shortage of sample; instead, they were estimated by extrapolating the  
50 linear trends between these values and concentration factors for the other PME3 samples, namely, PME3, PME3D1.3, PME3D2.5 and  
51 PME3D10.52 <sup>d</sup> Sodium could not be measured in the 2011 Davis fog samples due to high background sodium content .53 <sup>e</sup> Test statistic for comparison of standard PME and Davis fog averages: *p*-value for a two-tailed *t*-test for samples of unequal variance. Values  
54 below 0.05 are in bold.

55 **Table S3.** Hydroxyl radical measurements

Sample ID	$P_{OH}^a$ $10^{-10} \text{ M s}^{-1}$	$P_{OH}^a$ $\mu\text{M h}^{-1}$	$k'_{OH}^b$ $10^6 \text{ s}^{-1}$	$\tau_{OH}^c$ $\mu\text{s}$	$[\cdot\text{OH}]^d$ $10^{-16} \text{ M}$	$10^4 \times \Phi_{OH}^f$	$k'_{OH,org} / [\text{DOC}]^g$ $10^{-8} \text{ L (mol-C)}^{-1} \text{ s}^{-1}$
Particle Extracts							
PME1*	1.0 (0.1)	0.37 (0.04)	0.63 (0.01)	1.6 (0.1)	1.7 (0.2)	0.62 (0.06)	11.1 (0.2)
PME2*	2.0 (0.2)	0.71 (0.07)	0.44 (0.04)	2.3 (0.2)	4.5 (0.6)	1.1 (0.1)	4.6 (0.4)
PME3	14.7 (0.3)	5.3 (0.1)	2.3 (0.5)	0.46 (0.11)	6.4 (1.4) <sup>e</sup>	3.5 (0.1)	5.7 (1.3)
PME4	14 (2)	5.2 (0.6)	2.3 (0.2)	0.43 (0.03)	6.3 (0.6)	1.2 (0.1)	5.4 (0.4)
PME5	4.6 (0.5)	1.7 (0.2)	1.6 (0.1)	0.62 (0.03)	2.8 (0.3)	0.63 (0.07)	6.8 (0.4)
PME6	13 (3)	4.8 (1.0)	4.0 (0.8)	0.25 (0.05)	3.3 (0.3)	1.1 (0.2)	11 (2)
PME3D0.5					6.6 (1.6) <sup>e</sup>		
PME3D1.3					2.4 (0.6) <sup>e</sup>		
PME3D2.5*	3.1 (0.1)	1.1 (0.02)	1.3 (0.3)	0.78 (0.19)	2.3 (0.6) <sup>e</sup>	1.86 (0.03)	8.9 (2.2)
PME3D10	0.47 (0.04)	0.17 (0.01)	0.24 (0.02)	4.3 (0.3)	2.0 (0.5) <sup>e</sup>	1.1 (0.1)	6.1 (0.5)
Averages ( $\pm\sigma$ )							
“Standard” (PME3-6)	12 (5)	4.2 (1.7)	2.6 (1.0)	1.1 (0.2)	4.7 (1.9)	1.6 (1.3)	7.1 (2.5)
“Dilute” (PME1*- 2*,3D2.5*)	2.0 (1.0)	0.73 (0.37)	0.80 (0.84)	1.6 (0.8)	2.8 (1.5)	1.2 (0.6)	8.2 (3.3)
Davis Fog	3.5 (1.0)	1.3 (0.3)	0.87 (0.31)	1.2 (0.4)	4.2 (0.7)	2.4 (1.7)	7.5 (3.2)
Test statistic <sup>h</sup>	<b>0.039</b>	<b>0.039</b>	<b>0.042</b>	<b>0.042</b>	0.62	0.47	0.85
Field Blanks <sup>i</sup>							
FB1 (dilute)	$\leq 0.012$	$\leq 0.045$	0.34 (0.04)	3.0 (0.4)			
FB2 (standard)	$\leq 0.012$	$\leq 0.042$	0.27 (0.01)	3.8 (0.2)			

56 Listed uncertainties (in parentheses) are  $\pm 1$  standard error from the errors in inverse plot ( $1/R_p^*$  vs.  $1/[\text{Benzene}]$ ) parameters, except for the  
57 averages ( $\pm 1\sigma$ )

58 All equations used for these calculations are discussed in Kaur and Anastasio (2017) unless otherwise stated.

59 \* Samples extracted in 2.5 mL/filter square and referred to as the “dilute” extracts in the main text.

60 <sup>a</sup> Davis winter solstice-normalized rate of  $\cdot\text{OH}$  photoproduction.

61 <sup>b</sup> Apparent pseudo-first rate constant for destruction of  $\cdot\text{OH}$  due to natural sinks .

62 <sup>c</sup> Lifetime of  $\cdot\text{OH}$ , calculated as  $1/k'_{OH}$ .

63 <sup>d</sup> Winter solstice-normalized steady-state concentration of  $\cdot\text{OH}$ .

64 <sup>e</sup>  $\cdot\text{OH}$  concentrations in PME3 and PME3D extracts were measured using MBO as a probe (discussed in Sect. S1).

65 <sup>f</sup> Apparent quantum yield of  $\cdot\text{OH}$  during simulated sunlight illumination, calculated as  $\Phi_{OH} = P_{OH} / R_{abs}$ .

66 <sup>g</sup> Ratio of  $k'_{OH,org}$  (rate constant for loss of  $\cdot\text{OH}$  due to organics only; Table S6) to the DOC concentration.

67 <sup>h</sup> Test statistic for comparison of standard PME and Davis fog averages:  $p$ -value for a two-tailed  $t$ -test for samples of unequal variance. Values  
68 below 0.05 are in bold.

69 <sup>i</sup> Blanks were analyzed by adding 1.5 mM benzene to an aliquot of the blank. Very little phenol formation was observed after 200 minutes of  
70 illumination in both blanks, which was used to calculate the upper limit  $P_{OH}$ .

71 **Table S4.** Contributions of nitrite, nitrate and other sources to  $\cdot\text{OH}$  photoproduction

Sample ID	$f_{\text{POH,NO}_2^-}$ <sup>a</sup>	$f_{\text{POH,NO}_3^-}$ <sup>b</sup>	$f_{\text{POH,Other}}$ <sup>c</sup>
Particle Extracts			
PME1*	0.072 (0.010)	0.15 (0.02)	0.78 (0.02)
PME2*	0.36 (0.05)	0.63 (0.09)	0.011 (0.010)
PME3	0.18 (0.02)	0.24 (0.02)	0.58 (0.03)
PME4	0.15 (0.02)	0.32 (0.05)	0.53 (0.05)
PME5	0.21 (0.03)	0.11 (0.02)	0.67 (0.04)
PME6	0.11 (0.03)	0.046 (0.011)	0.85 (0.03)
PME3D0.5	-	-	-
PME3D1.3	-	-	-
PME3D2.5*	0.35 (0.04)	0.57 (0.06)	0.084 (0.068)
PME3D10	0.67 (0.08)	0.55 (0.07)	-0.22 (0.11) <sup>d</sup>
Averages ( $\pm\sigma$ )			
“Standard” (PME3-6)	0.16 (0.05)	0.18 (0.12)	0.66 (0.14)
“Dilute” (PME1*-2*,3D2.5*)	0.26 (0.16)	0.45 (0.26)	0.29 (0.42)
Davis Fog	0.24 (0.40)	0.46 (0.29)	0.41 (0.41)

72 Listed uncertainties (in parentheses) are  $\pm 1$  standard error calculated from propagating errors in individual terms, except for the averages ( $\pm 1\sigma$ ).

73 \* Samples extracted in 2.5 mL/filter square and referred to as the “dilute” extracts in the main text.

74 <sup>a</sup> Fraction of  $\cdot\text{OH}$  photoproduction rate attributable to nitrite. Calculated as  $(j_{\text{NO}_2 \rightarrow \text{OH}} \times [\text{NO}_2^-]) / P_{\text{OH}}$  where the numerator is the rate of  $\cdot\text{OH}$  photoproduction due  
75 to nitrite ( $P_{\text{OH,NO}_2}$ ), and is the product of the aqueous photolysis rate constant under Davis winter-solstice sunlight,  $j_{\text{NO}_2 \rightarrow \text{OH}} = 2.6 \times 10^{-5} \text{ s}^{-1}$  (Anastasio and  
76 McGregor, 2001), and the molar concentration of  $\text{NO}_2^-$  in each sample.

77 <sup>b</sup> Fraction  $\cdot\text{OH}$  photoproduction rate attributable to nitrate. Calculated using an equation analogous to  $f_{\text{POH,NO}_2^-}$ , using aqueous nitrate photolysis rate constant,  
78  $j_{\text{NO}_3^- \rightarrow \text{OH}} = 1.4 \times 10^{-7} \text{ s}^{-1}$  (Anastasio and McGregor, 2001) and molar concentration of  $\text{NO}_3^-$  in each sample.

79 <sup>c</sup> Fraction of  $\cdot\text{OH}$  photoproduction due to non-nitrite and -nitrate sources; calculated as  $(P_{\text{OH}} - P_{\text{OH,NO}_2^-} - P_{\text{OH,NO}_3^-}) / P_{\text{OH}}$ .

80 <sup>d</sup>  $f_{\text{POH,other}}$  is negative for PME3D10 indicating that the total rate of  $\cdot\text{OH}$  photoproduction is over-predicted using the measured molar  $\text{NO}_2^-$  and  $\text{NO}_3^-$   
81 concentrations.

82 **Table S5.** Determination of chloride as an  $\cdot\text{OH}$  sink, following procedure of Anastasio and Newberg (2007)

Sample ID	Measured $k'_{\text{OH}}^{\text{c}}$ $\text{s}^{-1}$	$[\text{Cl}^-]^{\text{d}}$ M	$[\text{H}^+]^{\text{e}}$ M	$f_{\text{Cl}^- \text{re-formed}}^{\text{f}}$	$k'_{\text{OH,Cl}^- \text{g}}$ $\text{s}^{-1}$	$f_{\text{KOH,Cl}^- \text{h}}$
PME1* <sup>a</sup>	6.3E+05	1.6E-05	6.31E-05	0.9997828	1.5E+01	2.3E-05
PME2* <sup>a</sup>	4.4E+05	2.0E-05	6.31E-05	0.99978	1.8E+01	4.2E-05
PME3	2.3E+06	6.6E-05	6.31E-05	0.99978	6.2E+01	2.9E-05
PME4	2.3E+06	7.0E-05	6.31E-05	0.99978	6.5E+01	2.8E-05
PME5	1.6E+06	3.7E-05	6.31E-05	0.999783	3.4E+01	2.1E-05
PME6	4.0E+06	7.8E-05	6.31E-05	0.99978	7.3E+01	1.8E-05
PME3D2.5* <sup>a</sup>	1.3E+06	2.7E-05	6.31E-05	0.99978	2.5E+01	2.0E-05
PME3D10 <sup>b</sup>	2.4E+05	6.9E-06	6.31E-05	0.999783	6.4E+00	2.8E-05

83 <sup>a</sup> Samples PME1\*, PME2\*, PME3D2.5 were extracted in 2.5 mL Milli-Q per filter square, and are referred to as “dilute extracts” in the main text.

84 <sup>b</sup> PME3D10 was extracted in 10 mL Milli-Q per filter square.

85 <sup>c</sup> Measured pseudo-first order rate constant for loss of  $\cdot\text{OH}$ .

86 <sup>d</sup> Measured chloride concentrations in the extracts.

87 <sup>e</sup> Hydrogen ion concentration. Since the extracts were acidified to pH 4.2, this value is constant across all extracts.

88 <sup>f</sup> Fraction of  $\text{Cl}^-$  reacting with  $\cdot\text{OH}$  that ends up back as  $\text{Cl}^-$  and  $\cdot\text{OH}$ . Values are calculated based on the reactions 1-4 below and the equation  $f_{\text{Cl}^- \text{re-formed}}$

89  $\text{re-formed} = k_4 / ((k_2 \times [\text{Cl}^-]) + (k_3 \times [\text{H}^+]) + k_4)$

90 <sup>g</sup> Rate constant for loss of  $\cdot\text{OH}$  due to  $\text{Cl}^-$  based on the fraction of reformed  $\text{Cl}^-$ , calculated as  $k'_{\text{OH,Cl}^-} = (1 - f_{\text{Cl}^- \text{re-formed}}) \times k_1$

91 <sup>h</sup> Fraction of measured  $k'_{\text{OH}}$  due to chloride.

92

93 (1)  $\cdot\text{OH} + \text{Cl}^- \rightarrow \text{HOCl}^{\cdot-}$   $k_1 = 4.3\text{E}+09 \text{ M}^{-1}\text{s}^{-1}$

94 (2)  $\text{HOCl}^{\cdot-} + \text{Cl}^- \rightarrow \cdot\text{Cl}_2^- + \text{OH}^-$ ,  $k_2 = 1.0\text{E}+04 \text{ M}^{-1}\text{s}^{-1}$

95 (3)  $\text{HOCl}^{\cdot-} + \text{H}^+ \rightarrow \text{Cl}^{\cdot} + \text{H}_2\text{O}$ ,  $k_3 = 2.1\text{E}+10 \text{ M}^{-1}\text{s}^{-1}$

96 (4)  $\text{HOCl}^{\cdot-} \rightarrow \text{Cl}^- + \cdot\text{OH}$ ,  $k_4 = 6.4\text{E}+09 \text{ M}^{-1}\text{s}^{-1}$



97 **Table S6.** Contributions of nitrite, chloride and organics to  $k'_{OH}$

Sample ID	Measured $k'_{OH}$ <sup>c</sup> s <sup>-1</sup>	$k'_{OH,NO_2^-}$ <sup>d</sup> s <sup>-1</sup>	$k'_{OH,Cl^-}$ <sup>e</sup> s <sup>-1</sup>	$k'_{OH,org}$ <sup>f</sup> s <sup>-1</sup>	$f_{k_{OH,NO_2^-}}$ <sup>g</sup>	$f_{k_{OH,org}}$ <sup>98</sup> <sub>h,i</sub>
PME1* <sup>a</sup>	6.3E+05	2.9E+03	1.5E+01	6.2E+05	0.0046	1.0
PME2* <sup>a</sup>	4.4E+05	2.7E+04	1.8E+01	4.1E+05	0.063	0.94
PME3	2.3E+06	1.0E+05	6.2E+01	2.1E+06	0.047	0.90
PME4	2.3E+06	8.3E+04	6.5E+01	2.2E+06	0.036	0.96
PME5	1.6E+06	3.8E+04	3.4E+01	1.6E+06	0.023	0.98
PME6	4.0E+06	5.4E+04	7.3E+01	4.0E+06	0.013	0.99
PME3D2.5* <sup>a</sup>	1.3E+06	4.1E+04	2.5E+01	1.2E+06	0.032	0.94
PME3D10 <sup>b</sup>	2.4E+05	1.2E+04	6.4E+00	2.2E+05	0.052	0.93

99 <sup>a</sup> Samples PME1\*, PME2\*, and PME3D2.5\* were extracted in 2.5 mL Milli-Q per filter square, and are referred to as “dilute extracts” in the main  
100 text.

101 <sup>b</sup> PME3D10 was extracted in 10 mL Milli-Q per filter square. All other extracts were extracted in 1.0 mL Milli-Q per filter square (standard  
102 extracts).

103 <sup>c</sup> Measured pseudo-first order rate constant for loss of  $\cdot OH$  (Table S3).

104 <sup>d</sup> Pseudo-first order rate constant for loss of  $\cdot OH$  due to nitrite. Value is calculated as  $k'_{OH,NO_2^-} = (k_{OH+NO_2^-} \times [NO_2^-])$  where  $k_{OH+NO_2^-} = 1.1 \times 10^{10} M^{-1}$   
105  $s^{-1}$  (Barker et al., 1970).

106 <sup>e</sup> Pseudo-first order rate constant for loss of  $\cdot OH$  due to chloride. Value is calculated using the reaction between  $\cdot OH$  and  $Cl^-$  corrected for the  
107 fraction of the initial product  $HOCl^{\cdot-}$  that fragments to reform  $\cdot OH$  and  $Cl^-$ , as discussed in Table S5 and Anastasio and Newberg (2007).

108 <sup>f</sup> Calculated pseudo-first-order rate constant for loss of  $\cdot OH$  due to organics, determined by subtracting the contribution of nitrite from the  
109 measured  $k'_{OH}$ . Contributions to  $k'_{OH}$  from common inorganic ions, including sulfate, nitrate, chloride, bicarbonate/carbonate (see footnote *h*  
110 below), and ammonium are negligible.

111 <sup>g</sup> Fraction of measured  $k'_{OH}$  due to nitrite.

112 <sup>h</sup> Fraction of measured  $\cdot OH$  sink due to organic species, estimated by subtracting the contributions due to nitrite from the measured value of  $k'_{OH}$ .

113 <sup>i</sup> The upper bound of the fraction of the measured  $k'_{OH}$  due to bicarbonate ( $HCO_3^-$ ) and carbonate ( $CO_3^{2-}$ ) was calculated to be  $1.1 \times 10^{-6}$  based on  
114 using the sample pH of 4.2 and assuming equilibrium with 400 ppm of atmospheric  $CO_2$ . This fraction was calculated based on the  $CO_2$   
115 equilibria 1-3 below (Seinfeld and Pandis, 2012),  $k_{OH+HCO_3^-} = 1 \times 10^7 M^{-1}s^{-1}$ , and  $k_{OH+CO_3^{2-}} = 4 \times 10^8 M^{-1}s^{-1}$  (Buxton et al., 1988b).

116 (1)  $CO_2 \leftrightarrow CO_2 \cdot H_2O(aq)$ ,  $K_{H^*} = 3.4E-02 M atm^{-1}$  (Physical Henry's law constant)

117 (2)  $CO_2 \cdot H_2O(aq) \leftrightarrow H^+ + HCO_3^-$ ,  $K_{a1} = 4.3E-07 M$  (pKa1 = 6.3)

118 (3)  $HCO_3^- \leftrightarrow H^+ + CO_3^{2-}$ ,  $K_{a2} = 4.7E-11 M$  (pKa2 = 10.3)

119 Thus, the contributions of  $HCO_3^-$  and  $CO_3^{2-}$  to measured  $k'_{OH}$  in all PME samples should be negligible.

**Table S7.** Singlet oxygen measurements

Sample ID	$P_{1O_2^*}^a$ $10^{-7} \text{ M s}^{-1}$	$P_{1O_2^*}^a$ $\mu\text{M h}^{-1}$	$[^1O_2^*]^b$ $10^{-12} \text{ M}$	$f_{\text{FFA},1O_2}^c$	$10^2 \times \Phi_{1O_2^*}^d$
Particle Extracts					
PME1*	0.36 (0.04)	131 (15)	0.16 (0.02)	0.51 (0.08)	2.2 (0.2)
PME2*	0.68 (0.06)	246 (20)	0.31 (0.03)	0.72 (0.07)	3.8 (0.3)
PME3	2.4 (0.2)	851 (81)	1.1 (0.1)	1.1 (0.1)	5.7 (0.5)
PME4	4.2 (0.4)	1515 (135)	1.9 (0.2)	1.0 (0.1)	3.4 (0.3)
PME5	2.8 (0.2)	1000 (59)	1.3 (0.1)	1.2 (0.1)	3.8 (0.2)
PME6	4.8 (0.3)	1719 (114)	2.2 (0.1)	1.1 (0.1)	3.8 (0.3)
PME3D0.5	3.9 (0.4)	1413 (138)	1.8 (0.2)	0.79 (0.10)	4.5 (0.4)
PME3D1.3	1.1 (0.1)	414 (40)	0.52 (0.05)	0.68 (0.07)	3.6 (0.3)
PME3D2.5*	0.55 (0.03)	198 (11)	0.25 (0.01)	0.61 (0.04)	3.3 (0.2)
PME3D10	0.14 (0.02)	50.8 (6.0)	0.064 (0.008)	0.59 (0.09)	3.3 (0.4)
Average ( $\pm\sigma$ )					
“Standard” (PME3-6)	3.5 (1.1)	1271 (412)	1.6 (0.5)	1.1 (0.1)	4.2 (1.0)
“Dilute” (PME1*-2*,3D2.5*)	0.53 (0.16)	192 (58)	0.24 (0.07)	0.61 (0.11)	3.1 (0.8)
Davis Fog	0.51 (0.14)	183 (49)	0.23 (0.06)	1.4 (0.8)	3.8 (3.1)
Test statistic <sup>f</sup>	<b>0.0064</b>	<b>0.0064</b>	<b>0.0064</b>		0.98
Field Blanks <sup>e</sup>					
FB1 (dilute)	$\leq 0.076$	$\leq 27$	$\leq 0.0034$		
FB2 (standard)	$\leq 0.069$	$\leq 25$	$\leq 0.0031$		

121

Listed uncertainties are  $\pm 1$  standard error unless otherwise stated.

122

All equations involved in the technique are discussed in Kaur and Anastasio (2017).

123

\* Samples extracted in 2.5 mL/filter square and referred to as the “dilute” extracts in the main text.

124

<sup>a</sup> Davis winter solstice-normalized rate of  $^1O_2^*$  formation.

125

<sup>b</sup> Davis winter solstice-normalized steady-state concentration of  $^1O_2^*$ .

126

<sup>c</sup> Fraction of probe FFA lost due to  $^1O_2^*$ .

127

<sup>d</sup> Apparent quantum yield of  $^1O_2^*$ , calculated as  $\Phi_{1O_2^*} = P_{1O_2^*} / R_{\text{abs}}$ .

128

<sup>e</sup> Blanks were analyzed by measuring FFA loss in undiluted blanks. This is an upper bound determined by ascribing all FFA loss to  $^1O_2^*$ .

129

<sup>f</sup> Test statistic for comparison of standard PME and Davis fog averages:  $p$ -value for a two-tailed  $t$ -test for samples of unequal variance. Values below 0.05 are in bold.

130

131 **Table S8.** Syringol loss kinetics

Sample ID	$k'_{\text{SYR}}^{\text{a}}$ $10^{-5} \text{ s}^{-1}$	$\tau_{\text{SYR}}^{\text{b}}$ h	$k'_{\text{SYR,OH}}^{\text{c}}$ $10^{-5} \text{ s}^{-1}$	$k'_{\text{SYR,IO}_2}^{\text{d}}$ $10^{-5} \text{ s}^{-1}$	$k'_{\text{SYR,3C}^*}^{\text{e}}$ $10^{-5} \text{ s}^{-1}$	$f_{\text{SYR,3C}^*}^{\text{f}}$
Particle Extracts						
PME1*	12 (1)	2.3 (0.3)	0.43 (0.04)	0.59 (0.07)	11 (1)	0.92 (0.15)
PME2*	14 (2)	2.0 (0.3)	1.2 (0.1)	1.1 (0.09)	11 (2)	0.83 (0.17)
PME3	33 (1)	0.85 (0.03)	1.7 (0.4)	3.9 (0.4)	27 (1)	0.83 (0.06)
PME4	69 (8)	0.40 (0.04)	1.6 (0.2)	6.9 (0.6)	61 (8)	0.88 (0.15)
PME5	35 (2)	0.80 (0.04)	0.74 (0.07)	4.5 (0.3)	29 (2)	0.85 (0.06)
PME6	37 (3)	0.74 (0.05)	0.85 (0.09)	7.8 (0.5)	24 (3)	0.77 (0.09)
PME3D0.5	48 (3)	0.58 (0.04)	1.7 (0.4)	6.4 (0.6)	40 (3)	0.83 (0.08)
PME3D1.3	26 (2)	1.1 (0.1)	0.63 (0.16)	1.9 (0.2)	24 (2)	0.90 (0.11)
PME3D2.5*	15 (2)	1.9 (0.3)	0.60 (0.15)	0.90 (0.05)	13 (2)	0.90 (0.19)
PME3D10	3.6 (0.4)	7.7 (0.8)	0.51 (0.14)	0.23 (0.03)	2.8 (0.4)	0.79 (0.14)
Average ( $\pm\sigma$ )						
“Standard” (PME3-6)	43 (17)	0.70 (0.20)	1.2 (0.5)	5.8 (1.9)	36 (16)	0.83 (0.05)
“Dilute” (PME1*- 2*,3D2.5*)	14 (1)	2.0 (0.2)	0.74 (0.39)	0.87 (0.26)	12 (1)	0.88 (0.04)
Davis Fog	16 (11)	2.4 (1.4)	1.1 (0.2)	0.83 (0.22)	14 (11)	0.85 (0.06)
Test statistic $^{\text{g}}$	<b>0.040</b>					
Field Blanks						
FB1 (dilute)	1.3 (0.2)	22 (3)				
FB2 (standard)	0.95 (0.07)	29 (2)				

132 Listed uncertainties are  $\pm 1$  standard error unless otherwise stated.

133 Bimolecular rate constants are given in Table S10.

134 \* Samples extracted in 2.5 mL/filter square and referred to as the “dilute” extracts in the main text.

135 <sup>a</sup> Davis winter-solstice-normalized value of the measured pseudo-first-order rate constant for loss of syringol (SYR).

136 <sup>b</sup> Lifetime of syringol, calculated as  $1/k'_{\text{SYR}}$ .

137 <sup>c</sup> Pseudo-first-order rate constant for loss of SYR due to hydroxyl radical, calculated as  $k'_{\text{SYR,OH}} = k_{\text{SYR+OH}} \times [\cdot\text{OH}]$ .

138 <sup>d</sup> Pseudo-first-order rate constant for loss of SYR due to singlet oxygen, calculated as  $k'_{\text{SYR,IO}_2} = k_{\text{SYR+IO}_2} \times [^1\text{O}_2^*]$ .

139 <sup>e</sup> Pseudo-first-order rate constant for loss of SYR due to triplet excited states, calculated as  $k'_{\text{SYR,3C}^*} = k'_{\text{SYR}} - (k'_{\text{SYR,OH}} + k'_{\text{SYR,IO}_2})$ .

140 <sup>f</sup> Fraction of SYR loss due to triplets, calculated as  $k'_{\text{SYR,3C}^*} / k'_{\text{SYR}}$ .

141 <sup>g</sup> Test statistic for comparison of standard PME and Davis fog averages:  $p$ -value for a two-tailed  $t$ -test for samples of unequal variance. Values below 0.05 are in  
142 bold.

**Table S9.** Methyl jasmonate loss kinetics

Sample ID	$k'_{\text{MeJA}}^a$ $10^{-5} \text{ s}^{-1}$	$\tau_{\text{MeJA}}^b$ h	$k'_{\text{MeJA,OH}}^c$ $10^{-5} \text{ s}^{-1}$	$k'_{\text{MeJA,1O2}}^d$ $10^{-5} \text{ s}^{-1}$	$k'_{\text{MeJA,3C}^*}^e$ $10^{-5} \text{ s}^{-1}$	$f_{\text{MeJA,3C}^*}^f$
Particle Extracts						
PME1*	0.98 (0.13)	28 (4)	0.11 (0.01)	0.099 (0.010)	0.77 (0.13)	0.79 (0.17)
PME2*	1.1 (0.1)	26 (1)	0.30 (0.04)	0.19 (0.02)	0.59 (0.07)	0.55 (0.07)
PME3	2.4 (0.2)	12 (1)	0.43 (0.01)	0.64 (0.06)	1.3 (0.2)	0.56 (0.10)
PME4	3.5 (0.4)	7.9 (0.8)	0.42 (0.04)	1.1 (0.1)	2.0 (0.4)	0.56 (0.12)
PME5	1.7 (0.2)	16 (2)	0.19 (0.02)	0.76 (0.04)	0.79 (0.18)	0.45 (0.11)
PME6	2.7 (0.2)	10 (1)	0.22 (0.02)	1.3 (0.1)	1.2 (0.2)	0.44 (0.08)
PME3D0.5	4.7 (0.5)	5.9 (0.7)	0.44 (0.11)	1.1 (0.1)	3.2 (0.6)	0.64 (0.14)
PME3D1.3	2.6 (0.2)	11 (1)	0.16 (0.04)	0.31 (0.03)	2.1 (0.3)	0.82 (0.12)
PME3D2.5*	1.8 (0.2)	16 (2)	0.16 (0.04)	0.15 (0.01)	1.5 (0.2)	0.83 (0.15)
PME3D10	0.67 (0.09)	42 (5)	0.13 (0.04)	0.038 (0.005)	0.50 (0.09)	0.74 (0.17)
Average ( $\pm\sigma$ )						
“Standard” (PME3-6)	2.6 (0.7)	11 (3)	0.31 (0.13)	0.96 (0.31)	1.3 (0.5)	0.50 (0.06)
“Dilute” (PME1*- 2*,3D2.5*)	1.3 (0.4)	23 (7)	0.19 (0.10)	0.15 (0.04)	0.94 (0.46)	0.72 (0.15)
Davis Fog	0.90 (0.12)	31 (4)	0.28 (0.05)	0.14 (0.04)	0.48 (0.17)	0.53 (0.13)
Test statistic <sup>g</sup>	<b>0.018</b>					
Field Blanks						
FB1 (dilute)	0.17 (0.2)	160 (18)				
FB2 (standard)	0.27 (0.08)	104 (31)				

144

Listed uncertainties are  $\pm 1$  standard error unless otherwise stated.

145

Bimolecular rate constants are given in Table S10.

146

\* Samples extracted in 2.5 mL/filter square and referred to as the “dilute” extracts in the main text.

147

<sup>a</sup> Davis winter-solstice-normalized measured pseudo-first-order rate constant for loss of methyl jasmonate (MeJA).

148

<sup>b</sup> Lifetime of methyl jasmonate, calculated as  $1/k'_{\text{MeJA}}$ .

149

<sup>c</sup> Pseudo-first-order rate constant for loss of MeJA due to hydroxyl radical, calculated as  $k'_{\text{MeJA,OH}} = k_{\text{MeJA+OH}} \times [\cdot\text{OH}]$ .

150

<sup>d</sup> Pseudo-first-order rate constant for loss of MeJA due to singlet oxygen, calculated as  $k'_{\text{MeJA,1O2}} = k_{\text{MeJA+1O2}} \times [^1\text{O}_2^*]$ .

151

<sup>e</sup> Pseudo-first-order rate constant for loss of MeJA due to triplet excited states, calculated as  $k'_{\text{MeJA,3C}^*} = k'_{\text{MeJA}} - (k'_{\text{MeJA,OH}} + k'_{\text{MeJA,1O2}})$ .

152

<sup>f</sup> Fraction of MeJA loss due to triplets, calculated as  $k'_{\text{MeJA,3C}^*} / k'_{\text{MeJA}}$ .

153

<sup>g</sup> Test statistic for comparison of standard PME and Davis fog averages:  $p$ -value for a two-tailed  $t$ -test for samples of unequal variance. Values below 0.05 are in bold.

154

155 **Table S10.** Second-order rate constants for reactions of syringol and methyl jasmonate with hydroxyl radical, singlet oxygen, and triplet  
 156 excited states

Oxidants	$k_{\text{SYR}+\text{Oxidant}}$ $10^9 \text{ M}^{-1} \text{ s}^{-1}$	Reference	$k_{\text{MeJA}+\text{Oxidant}}$ $10^8 \text{ M}^{-1} \text{ s}^{-1}$	Reference	
$\cdot\text{OH}$	26	O'Neill and Steenken (1977)	67 ( $\pm 3$ )	Richards-Henderson et al. (2014a)	
$^1\text{O}_2^*$	0.0036	Tratnyek and Hoigne (1991b)	0.0060 ( $\pm 0.0007$ )	Richards-Henderson et al. (2014b)	
Model Triplets ( $^3\text{C}^*$ )					$k_{\text{SYR}+3\text{C}^*}/k_{\text{MeJA}+3\text{C}^*}$ <sup>a</sup>
$^3\text{2AN}^*$	1.9 ( $\pm 0.1$ )	Kaur and Anastasio (2018)	0.19 ( $\pm 0.07$ )	Kaur and Anastasio (2018)	100 ( $\pm 37$ )
$^3\text{3MAP}^*$	3.8 ( $\pm 0.6$ )	Kaur and Anastasio (2018)	1.2 ( $\pm 0.3$ )	Richards-Henderson et al. (2014b)	32 ( $\pm 9$ )
$^3\text{DMB}^*$	3.5 ( $\pm 0.8$ )	Smith et al. (2015)	4.1 ( $\pm 1.6$ )	Richards-Henderson et al. (2014b)	8.5 ( $\pm 3.8$ )
$^3\text{BP}^*$	8.5 ( $\pm 1.6$ )	Kaur and Anastasio (2018)	51 ( $\pm 9$ )	Kaur and Anastasio (2018)	1.7 ( $\pm 0.4$ )

157 Listed uncertainties are  $\pm 1$  standard error.

158 <sup>a</sup> Ratio of the bimolecular rate constants for reaction of a given model triplet with syringol (SYR) and methyl jasmonate (MeJA).

159 **Table S11.** Characteristics of model triplet species

Model Triplet	$E_T^a$ (kJ mol <sup>-1</sup> )	$E^{0*}({}^3C^*/C^{\cdot-})^b$ (V)	$k_{O_2+{}^3C^*}^c$ (10 <sup>9</sup> ) M <sup>-1</sup> s <sup>-1</sup>	$f_\Delta^d$
<sup>3</sup> 2AN*	249	1.10	2.5	0.81 (C <sub>6</sub> H <sub>6</sub> )
<sup>3</sup> 3MAP*	303	1.64	3.3	0.33 (C <sub>6</sub> H <sub>6</sub> )
<sup>3</sup> DMB*	298 (estimated) <sup>e</sup>	-	-	< 0.61 (MeOH) (estimated) <sup>e</sup>
<sup>3</sup> BP*	288	1.67	2.6	0.35 (C <sub>6</sub> H <sub>6</sub> )

160 All values from Canonica et al.(Cannonica et al., 2000) and Wilkinson et. al.(Wilkinson et al., 1993)

161 <sup>a</sup> Triplet state energy (T<sub>1</sub>→ S<sub>0</sub>).

162 <sup>b</sup> One-electron reduction potential for the triplet/triplet radical anion pair.

163 <sup>c</sup> Bimolecular rate constant for quenching of triplet by molecular O<sub>2</sub>. To calculate rates of triplet photoformation (described in the main text), an  
164 average value of 2.8 (± 0.4) × 10<sup>9</sup> M<sup>-1</sup>s<sup>-1</sup> is used.

165 <sup>d</sup> Yield of singlet oxygen from quenching of model triplet species by O<sub>2</sub>. The solvent used in the determination is indicated in parentheses. Including  
166 the upper-bound value of 0.61 for <sup>3</sup>DMB\* (discussed in footnote *e*), the average value of  $f_\Delta$  for the model triplets is 0.53 (± 0.23).

167 <sup>e</sup> Since the  $E_T$  and  $f_\Delta$  values for <sup>3</sup>DMB\* are not available, values for benzaldehyde (Hunter, 1970; Wilkinson et al., 1993) are used as estimates. The  $f_\Delta$   
168 value is an upper-bound estimate.  
169

170 **Table S12.** Best triplet matches and best estimate triplet steady-state concentrations

Sample ID	$k'_{\text{SYR},3\text{C}^*} / k'_{\text{MeJA},3\text{C}^*}$ <sup>a</sup>	Mole-fractions of Best Triplet Matches <sup>b</sup>				Bimolecular rate constants ( $\text{M}^{-1} \text{s}^{-1}$ ) $\chi_{3\text{C}1^*} \times k_{\text{Probe}+3\text{C}1^*} + \chi_{3\text{C}2^*} \times k_{\text{Probe}+3\text{C}2^*}$ <sup>c</sup>			Triplet Steady-State Concentration ( $10^{-14} \text{ M}$ )		
		<sup>3</sup> 2AN*	<sup>3</sup> 3MAP*	<sup>3</sup> DMB*	<sup>3</sup> BP*	SYR	MeJA	SYR/MeJA Ratio	$\Sigma[{}^3\text{C}_i^*]_{\text{SYR}}$ <sup>d</sup>	$\Sigma[{}^3\text{C}_i^*]_{\text{MeJA}}$ <sup>e</sup>	$\Sigma[{}^3\text{C}_i^*]$ ( $\pm 1\text{S.E.}$ ) Best Estimate <sup>f,g</sup>
PME1*	15 (3)		0.55	0.45		3.7E+09	2.5E+08	15	3.1	3.1	3.1 (1.2)
PME2*	20 (4)		0.76	0.24		3.7E+09	1.9E+08	20	3.1	3.1	3.1 (1.0)
PME3	20 (3)		0.78	0.22		3.7E+09	1.9E+08	20	7.3	7.3	7.3 (2.2)
PME4	30 (7)		0.98	0.02		3.8E+09	1.3E+08	30	16	16	16 (5)
PME5	37 (8)	0.34	0.66			3.2E+09	8.5E+07	37	9.3	9.3	9.3 (3.1)
PME6	24 (4)		0.86	0.14		3.8E+09	1.6E+08	24	7.7	7.7	7.7 (2.2)
PME3D0.5	13 (2)		0.42	0.59		3.6E+09	2.9E+08	13	11	11	11 (4)
PME3D1.3	11 (2)		0.30	0.70		3.6E+09	3.2E+08	11	6.6	6.6	6.6 (2.7)
PME3D2.5*	9.2 (2.0)		0.09	0.91		3.5E+09	3.8E+08	9.2	3.8	3.8	3.8 (1.8)
PME3D10	5.7 (1.4)			0.95	0.05	3.8E+09	6.6E+08	5.7	0.76	0.76	0.76 (0.30)

171 Uncertainties in parentheses are  $\pm 1$  standard error.

172 Details of the technique are discussed in Kaur and Anastasio (2018).

173 \* Samples extracted in 2.5 mL/filter square and referred to as the “dilute” extracts in the main text.

174 <sup>a</sup> Ratio of measured values of  $k'_{\text{Probe},3\text{C}^*}$  in a given particle extract.

175 <sup>b</sup> Mole fractions of model triplets whose  $k_{\text{Probe}+3\text{C}^* \text{Model}}$  ratio lies closest to the  $k'_{\text{Probe},3\text{C}^*}$  ratio in each sample.

176 <sup>c</sup> Mole-fraction-weighted bimolecular rate constants for both probes.

177 <sup>d</sup> Triplet steady-state concentration calculated from syringol loss as  $k'_{\text{SYR},3\text{C}^*} / (\chi_{3\text{C}1^*} k_{\text{SYR}+3\text{C}1^*} + \chi_{3\text{C}2^*} k_{\text{SYR}+3\text{C}2^*})$

178 <sup>e</sup> Triplet steady-state concentration calculated from methyl jasmonate loss as  $k'_{\text{MeJA},3\text{C}^*} / (\chi_{3\text{C}1^*} k_{\text{MeJA}+3\text{C}1^*} + \chi_{3\text{C}2^*} k_{\text{MeJA}+3\text{C}2^*})$

179 <sup>f</sup> Best estimate steady-state concentration calculated as the average of the  $\Sigma[{}^3\text{C}_i^*]_{\text{SYR}}$  and  $\Sigma[{}^3\text{C}_i^*]_{\text{MeJA}}$ .

180 <sup>g</sup> Uncertainties in parentheses are  $\pm 1$  SE propagated from the errors of  $k'_{\text{SYR},3\text{C}^*}$  and  $k'_{\text{MeJA},3\text{C}^*}$  and the mole-fraction-weighted bimolecular rate constants. Values are  
181 shown in Tables S8 and S9.

182 **Table S13.** Measurements of triplet excited states of organic matter

Sample ID	$\Sigma[{}^3C_i^*]$ Best Estimate <sup>a</sup> $10^{-14}$ M	$P_{3C^*}$ <sup>b</sup> $10^{-7}$ M s <sup>-1</sup>	$P_{3C^*}$ <sup>b</sup> $\mu$ M h <sup>-1</sup>	$10^2 \times \Phi_{3C^*}$ <sup>c</sup>	$\frac{\Phi_{3C^*}}{(\Phi_{1O_2^*}/f_{\Delta})}$ <sup>d</sup> *	$\frac{\Sigma[{}^3C_i^*]}{[{}^1O_2^*]}$ <sup>e</sup>
Particle Extracts						
PME1*	3.1 (1.2)	0.30 (0.13)	109 (48)	1.8 (0.8)	0.44 (0.20)	0.19 (0.07)
PME2*	3.1 (1.0)	0.34 (0.13)	122 (47)	1.9 (0.7)	0.26 (0.10)	0.10 (0.03)
PME3	7.3 (2.2)	1.5 (0.5)	530 (195)	3.5 (1.3)	0.33 (0.13)	0.068 (0.021)
PME4	16 (5)	3.5 (1.4)	1260 (501)	2.8 (1.1)	0.44 (0.18)	0.083 (0.029)
PME5	9.3 (3.1)	1.5 (0.6)	534 (211)	2.0 (0.8)	0.28 (0.11)	0.074 (0.025)
PME6	7.7 (2.2)	1.6 (0.6)	568 (206)	1.3 (0.5)	0.18 (0.06)	0.035 (0.011)
PME3D0.5	11 (4)	3.6 (1.6)	1281 (587)	4.1 (1.9)	0.48 (0.23)	0.062 (0.026)
PME3D1.3	6.6 (2.7)	1.1 (0.5)	411 (192)	3.6 (1.7)	0.53 (0.25)	0.13 (0.05)
PME3D2.5*	3.8 (1.8)	0.48 (0.26)	174 (92)	2.9 (1.5)	0.46 (0.25)	0.15 (0.07)
PME3D10	0.76 (0.30)	0.0069 (0.0031)	25 (11)	1.6 (0.7)	0.26 (0.12)	0.12 (0.05)
Averages ( $\pm\sigma$ )						
“Standard” (PME3-6)	10 (4)	2.0 (1.0)	722 (356)	2.4 (1.0)	0.31 (0.11)	0.065 (0.021)
“Dilute” (PME1*- 2*,3D2.5*)	3.3 (0.4)	0.38 (0.01)	135 (34)	2.2 (0.6)	0.39 (0.11)	0.15 (0.04)
Davis Fog	5.4 (6.3)	0.59 (0.60)	212 (216)	5.8 (8.6)	0.55 (0.44)	0.21 (0.20)
Test statistic <sup>f</sup>	0.27	<b>0.059</b>	<b>0.059</b>	0.49	0.35	0.25

183 Listed uncertainties are  $\pm 1$  standard error.

184 \* Samples extracted in 2.5 mL/filter square and referred to as the “dilute” extracts in the main text.

185 <sup>a</sup> Best estimate of oxidizing triplets steady-state concentration, calculated as the average of the  $\Sigma[{}^3C_i^*]_{\text{SYR}}$  and  $\Sigma[{}^3C_i^*]_{\text{MeJA}}$  values, as shown in Table S12.

186 <sup>b</sup> Davis winter solstice-normalized rate of triplet photoproduction, calculated as  $P_{3C^*} = \Sigma[{}^3C_i^*] \times (k_{3C^*+O_2} \times [O_2] + (k_{\text{rxn}} + k_Q)[\text{DOC}])$  (Eq. (8), main text).

187 <sup>c</sup> Quantum yield for formation of oxidizing organic triplet excited states, calculated as  $\Phi_{3C^*} = P_{3C^*} / R_{\text{abs}}$ .

188 <sup>d</sup> Fraction of the total triplet pool that can oxidize our probes, i.e., that are “oxidizing triplets”. This is estimated as the ratio of the quantum yields for oxidizing  
 189 triplets and singlet oxygen (Table S7) divided by the average yield of  ${}^1O_2^*$  ( $f_{\Delta} = 0.53$ ; Table S11) from  ${}^3C^*$  via energy transfer. The denominator,  $\Phi_{1O_2^*}/f_{\Delta}$ , is an  
 190 estimate of the quantum yield for formation of energy-transfer triplets that can make singlet molecular oxygen, a pool that likely includes essentially all organic  
 191 triplet states.

192 <sup>e</sup> Ratio of the Davis-winter-normalized steady-state triplet and singlet oxygen concentrations.



193 <sup>f</sup> Test statistic for comparison of standard PME and Davis fog averages:  $p$ -value for a two-tailed  $t$ -test for samples of unequal variance. Values below 0.05 are in  
194 bold.



196 **Table S14.** Particle mass to water mass ratios in the PME3 extracts, typical fog drops, and particles

Sample ID	Number of filter squares extracted	Volume of Milli-Q water per filter square (mL) <sup>a</sup>	Aqueous PM mass concentration factor (CF) <sup>b</sup>	Average PM mass extracted per filter square (μg) <sup>c</sup>	Total PM mass extracted (μg) <sup>d</sup>	Total volume of extract (mL) <sup>e</sup>	PM mass / water mass (μg-PM / μg-H <sub>2</sub> O) <sup>f</sup>
PME3D10	1	10	0.05	347	347	10	3.5E-05
PME3D2.5	12	2.5	0.20	331 (15)	3977	30	1.3E-04
PME3D1.3	8	1.3	0.38	315 (23)	2520	10	2.4E-04
PME3D1 or “PME3”	12	1.0	0.49	328 (19)	3932	12	3.3E-04
PME3D0.5	26	0.5	0.96	323 (21)	10979	13	8.4E-04
Cloud/Fog drop							(1 – 5)E-04 <sup>g</sup>
Particles							≥ 1 <sup>h</sup>

197 <sup>a</sup> Volume of water used to extract each 2 × 2 cm square piece of the filter sheet.

198 <sup>b</sup> PM mass concentration factor in the extract (Eq. (10), main text).

199 <sup>c</sup> Average (± 1σ) mass extracted from the filter squares for each dilution.

200 <sup>d</sup> Total mass extracted per extract. For each extract, the filter pieces used in the extraction were weighed pre- and post-extraction using a Mettler Toledo XP2U ultra-  
201 microbalance (error ± 2 μg). The PM mass extracted is the difference between pre- and post-extraction weights.

202 <sup>e</sup> Total volume of extract = number of filter pieces extracted × water volume per filter square.

203 <sup>f</sup> PM mass-to-water mass ratio, calculated as total mass extracted / total volume of extract.

204 <sup>g</sup> For fog drops, we estimate that PM mass/water mass ratios are in the range of (1 – 5) × 10<sup>-4</sup> μg-PM/μg-H<sub>2</sub>O based on a typical PM mass of 31 μg m<sup>-3</sup>-air in  
205 California’s Central Valley, as measured by Young et al. (2016), and assuming a range for the liquid water content (LWC) of 0.06 to 0.3 g-H<sub>2</sub>O m<sup>-3</sup>-air (Hess et  
206 al., 1998).

207 <sup>h</sup> Based on measurements of particle mass (Young et al. (2016)) and particle water (Parworth et al., 2017) in California’s Central Valley during winter, the calculated  
208 range of PM mass to water mass ratios is 0.79 – 50. From this range, we use a value of 1 to represent typical PM conditions.

209 **Table S15.** Photooxidant concentrations (formed *in situ*) in PME3D extracts and expected values in ambient particles

Sample ID	Aqueous PM Mass Concentration Factor (CF) <sup>a</sup>	PM Mass /Water Mass ( $\mu\text{g-PM}/\mu\text{g-H}_2\text{O}$ ) <sup>b</sup>	[ $\cdot\text{OH}$ ] (M)	[ $^1\text{O}_2^*$ ] (M)	$\Sigma[{}^3\text{C}_i^*]$ (M)
PME3D10	0.05	3.5E-05	2.0E-16	6.4E-14	7.6E-15
PME3D2.5*	0.20	1.3E-04	2.3E-16	2.5E-13	3.8E-14
PME3D1.3	0.38	2.4E-04	2.4E-16	5.2E-13	6.6E-14
PME3D1	0.49	3.3E-04	6.3E-16	1.1E-12	7.3E-14
PME3D0.5	0.96	8.4E-04	6.5E-16	1.8E-12	1.1E-13
Ambient Particles		1.0	3.9E-16 <sup>c</sup>	2.2E-09 <sup>d</sup>	1.7E-13 <sup>e</sup> 1.5E-10 <sup>f</sup>

210 <sup>a</sup> Aqueous PM mass concentration factor (Eq. (10), main text).

211 <sup>b</sup> PM mass/water mass ratio (Table S14).

212 <sup>c</sup> Expected *in situ* [ $\cdot\text{OH}$ ] concentration in ambient PM (in the absence of partitioning of  $\cdot\text{OH}$  from the gas phase), determined as the average of the five measurements  
213 in PME3D extracts. Including mass transport of  $\cdot\text{OH}(\text{g})$  to the drops will increase the aqueous concentration by approximately 30%, as discussed in the text.

214 <sup>d</sup> Expected [ $^1\text{O}_2^*$ ] concentration in ambient PM (in the absence of volatilization of  $^1\text{O}_2^*$  from the particles), extrapolated using the slope of the plot of [ $^1\text{O}_2^*$ ] v. PM  
215 mass/water mass ratio. Including volatilization would decrease the aqueous concentration of  $^1\text{O}_2^*$  by half.

216 <sup>e</sup> Expected lower bound for the  $\Sigma[{}^3\text{C}_i^*]$  concentration in ambient PM, obtained by plotting  $\Sigma[{}^3\text{C}_i^*]$  against PM mass/water mass ratio, fitting the data to the two-  
217 parameter equation  $ax/(1+bx)$ ; parameters  $a = 4.0 \times 10^{-10}$  and  $b = 2.4 \times 10^3$  were obtained using Sigmaplot 12.0. The curve was then extrapolated to a PM  
218 mass/water mass ratio of  $1.0 \mu\text{g-PM}/\mu\text{g-H}_2\text{O}$ .

219 <sup>f</sup> Expected upper bound for the  $\Sigma[{}^3\text{C}_i^*]$  concentration in ambient PM, obtained by extrapolating the linear plot of  $\Sigma[{}^3\text{C}_i^*]$  against PM mass/water mass ratio to a ratio  
220 of  $1.0 \mu\text{g-PM}/\mu\text{g-H}_2\text{O}$ .

221 **Table S16.** Gas- and aqueous-phase reaction rate constants for selected organic compounds with the major oxidants

#	Organic Compound	Gas-phase rate constant, $k_{\text{ORG}+\text{Ox}(\text{g})}$ ( $\text{cm}^3 \text{mlc}^{-1} \text{s}^{-1}$ )				Aqueous-phase rate constants, $k_{\text{ORG}+\text{Ox}(\text{aq})}$ ( $\text{M}^{-1} \text{s}^{-1}$ )							
		$\bullet\text{OH}(\text{g})$	Ref.	$\text{O}_3(\text{g})$	Ref.	$\bullet\text{OH}(\text{aq})$	Ref.	$^1\text{O}_2^*(\text{aq})$	Ref.	$\text{O}_3(\text{aq})$	Ref.	$^3\text{C}^*(\text{aq})^a$	Ref.
1	Syringol	9.6E-11	(Lauraguais et al., 2012)	4.0E-19 <sup>b</sup>	(Zein et al., 2015)	2.6E+10	(O'Neill and Steenken, 1977)	3.6E+07	(Tratnyek and Hoigne, 1991a)	1.3E+04 <sup>c</sup>	(Hoigné and Bader, 1983)	3.7E+09	(Kaur and Anastasio, 2018), (Smith et al., 2015)
2	Methyl jasmonate	7.8E-12 <sup>d</sup>	(Meylan and Howard, 1993)	1.7E-16 <sup>d</sup>	(Meylan and Howard, 1993)	6.7E+09	(Richards-Henderson et al., 2014a)	6.0E+06	(Richards-Henderson et al., 2014c)	1.0E+05 <sup>e</sup>	(Richards-Henderson et al., 2014c)	2.7E+08	(Kaur and Anastasio, 2018)
3	Tyrosine	2.8E-11 <sup>f</sup>	(Rinke and Zetzsch, 1984)	4.7E-19 <sup>g</sup>	(Atkinson et al., 1982)	1.3E+10	(Solar et al., 1984)	3.8E+07	(Bertolotti et al., 1991)	3.3E+05 (pH 4.2)	(McGregor and Anastasio, 2001)	6.6E+08 <sup>h</sup>	(Canonica et al., 2000)
4	1,2,4-Butanetriol	8.5E-12 <sup>i</sup>	(Atkinson et al., 2006)	1.0E-20 <sup>j</sup>	(Atkinson et al., 2006)	5.0E+09 <sup>k</sup>	(Anbar et al., 1966)	6.0E+04 <sup>l</sup>	(Wilkinson et al., 1995)	2 <sup>m</sup>	(Hoigné and Bader, 1983)	1.1E+06 <sup>n</sup>	(Tetreau et al., 1972)
5	3-Hydroxy-2,5-bis(hydroxymethyl) furan	4.0E-11 <sup>o</sup>	(Atkinson et al., 1983)	2.4E-18 <sup>o</sup>	(Atkinson et al., 1983)	3.9E+09 <sup>p</sup>	(Lilie, 1971)	1.0E+08 <sup>q</sup>	(Wilkinson et al., 1995)	1.2E+03 <sup>r</sup>	(Andreev, 2012)	1.4E+08 <sup>s</sup>	(Kaur and Anastasio, 2018)

222 References for the measured rate constants are indicated. Values indicated are at 298 K wherever available. In cases where no measurements were found, rate  
 223 constants for structurally similar compounds are used as proxies; references for those are provided, and discussed in the following footnotes.

224 <sup>a</sup> For triplets, we use an average of rate constants for <sup>3</sup>MAP\* and <sup>3</sup>DMB\*.

225 <sup>b</sup> Second-order rate constant for the gas-phase reaction of O<sub>3</sub> with guaiacol (2-methoxyphenol).

226 <sup>c</sup> Second-order rate constant for the aqueous reaction of O<sub>3</sub> with phenol is used as a proxy, with a ten-fold enhancement based on the measured ratio of phenol and  
 227 syringol rate constants for reaction with <sup>3</sup>DMB\* (discussed in the SI of Kaur and Anastasio (2018)).

228 <sup>d</sup> Average of cis- and trans-methyl jasmonate rate constants with hydroxyl radical and ozone.

229 <sup>e</sup> Estimated by Richards-Henderson et al. (2014c) using a structurally similar compound.

230 <sup>f</sup> Second-order rate constant for the aqueous-phase reaction of O<sub>3</sub> with phenol.

231 <sup>g</sup> Second-order rate constant for the aqueous-phase reaction of O<sub>3</sub> with 3-methylphenol.

232 <sup>h</sup> Second-order rate constant for aqueous-phase reaction of tyrosine with 3'-methoxyacetophenone.

233 <sup>i</sup> Second-order rate constant for gas-phase reaction of  $\bullet\text{OH}$  with 1-butanol.

234 <sup>j</sup> Second-order rate constant for gas-phase reaction of O<sub>3</sub> with pinonaldehyde.

235 <sup>k</sup> Second-order rate constant for aqueous-phase reaction of  $\bullet\text{OH}$  with 1,6-hexanediol.

236 <sup>l</sup> Second-order rate constant for aqueous-phase reaction of <sup>1</sup>O<sub>2</sub>\* with 2-butanol.

237 <sup>m</sup> Second-order rate constant for aqueous-phase reaction of O<sub>3</sub> with 2-propanol.

238 <sup>n</sup> Second-order rate constant for aqueous-phase reaction of <sup>3</sup>DMB\* with 2-propanol.

239 <sup>o</sup> Second-order rate constant for gas-phase reaction of  $\bullet\text{OH}$  and O<sub>3</sub> with furan.

240 <sup>p</sup> Second-order rate constant for aqueous-phase reaction of  $\bullet\text{OH}$  with furan.

241 <sup>q</sup> Second-order rate constant for aqueous-phase reaction of <sup>1</sup>O<sub>2</sub>\* with furan, adjusted by multiplying with 0.5 based on effect of changing substituents.

242 <sup>r</sup> Second-order rate constant for aqueous-phase reaction of O<sub>3</sub> with furan in glacial acetic acid.

243 <sup>s</sup> Average of the second-order rate constant for aqueous-phase reaction of <sup>3</sup>MAP\* and <sup>3</sup>DMB\* with methyl jasmonate is used a proxy, adjusted by multiplying with  
 244 0.5 based on effect of changing substituents observed for rate constant of furan with <sup>1</sup>O<sub>2</sub>\*.

245 **Table S17.** Fate of selected organic compounds in fog and particles

#	Organic Compound	$K_H^a$ (M atm <sup>-1</sup> )	$f_{aq}^b$	Overall		Percent of loss due to each oxidant <sup>e</sup>					
				$k'_{ORG}^c$ (s <sup>-1</sup> )	$\tau_{ORG}^d$ (h)	$\bullet OH(g)$	O <sub>3</sub> (g)	$\bullet OH(aq)$	<sup>1</sup> O <sub>2</sub> *(aq)	O <sub>3</sub> (aq)	<sup>3</sup> C*(aq)
<b>Fog</b>											
1	Syringol	5.0E+03	0.11	1.1E-04	2.5	76	0	5	1	0	18
2	Methyl jasmonate	8.1E+03	0.17	1.2E-04	2.3	5	86	2	0	5	2
3	Tyrosine	8.0E+10	1.0	1.8E-04	1.6	0	0	15	4	62	19
4	1,2,4-Butanetriol	4.7E+11	1.0	1.0E-05	28	0	0	99	0	0	0
5	3-Hydroxy-2,5-bis(hydroxymethyl) furan	1.1E+09	1.0	3.5E-05	7.9	0	0	22	57	1	19
<b>PM (Lower-bound [<sup>3</sup>C*] scenario)</b>											
1	Syringol	5.0E+03	2.4E-06	9.6E-05	2.9	100	0	0	0	0	0
2	Methyl jasmonate	8.1E+03	4.0E-06	1.3E-04	2.1	6	94	0	0	0	0
3	Tyrosine	8.0E+10	0.98	5.8E-03	0.048	0	0	0	96	2	2
4	1,2,4-Butanetriol	4.7E+11	1.0	1.9E-05	15	0	0	52	47	0	1
5	3-Hydroxy-2,5-bis(hydroxymethyl) furan	1.1E+09	0.35	5.3E-03	0.053	0.5	0	0.1	99	0.0	0.2
<b>PM (Upper-bound [<sup>3</sup>C*] scenario)</b>											
1	Syringol	5.0E+03	2.4E-06	9.8E-05	2.8	98	0	0	0	0	1
2	Methyl jasmonate	8.1E+03	4.0E-06	1.3E-04	2.1	6	94	0	0	0	0
3	Tyrosine	8.0E+10	0.98	1.0E-01	0.0027	0	0	0	5	0	94
4	1,2,4-Butanetriol	4.7E+11	1.0	1.7E-04	1.7	0	0	6	5	0	89
5	3-Hydroxy-2,5-bis(hydroxymethyl) furan	1.1E+09	0.35	1.2E-02	0.022	0	0	0	42	0	57

246 For fog, a liquid water content of  $1 \times 10^{-6}$  L-aq / L-air is assumed.

247 For PM, a liquid water content of  $2 \times 10^{-11}$  L-aq / L-air is assumed, based on typical wintertime Central Valley conditions (Parworth et al., 2017).

248 <sup>a</sup> Henry's law constant estimated using EPISuite version 4.11 (USEPA, 2012). For methyl jasmonate, measured value from Vempati (2014).

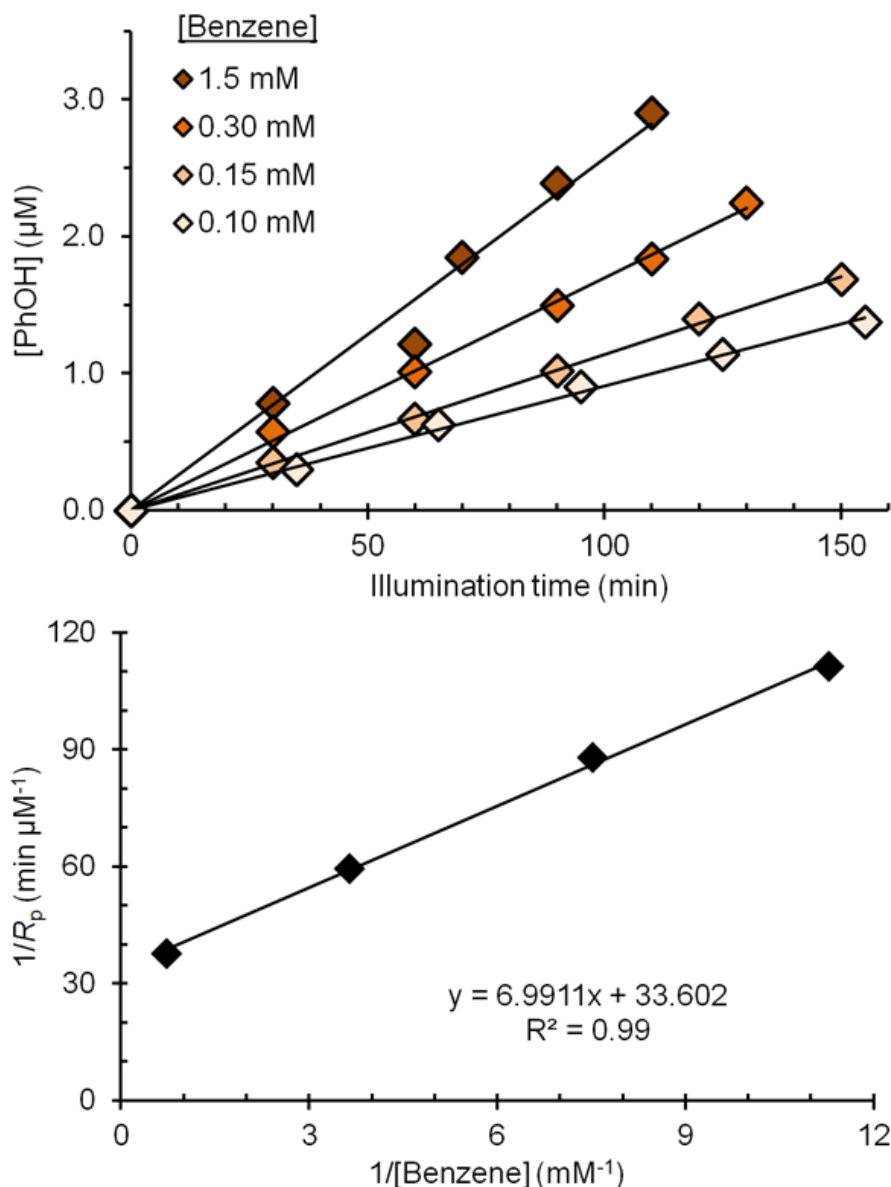
249 <sup>b</sup> Fraction of organic compound present in the aqueous-phase, calculated as  $f_{aq} = 1/(1+1/(K_H \times L \times R \times T))$ , where  $K_H$  is the Henry's law constant,  $L$  is the liquid water content,  $R$  is the gas constant (0.082 L atm K<sup>-1</sup> mol<sup>-1</sup>), and  $T = 298$  K.

251 <sup>c</sup> Total pseudo-first order rate constant for loss of organic compound, calculated as  $k'_{ORG} = \Sigma(f_{aq} \times k'_{ORG,Ox(aq)} + (1-f_{aq}) \times k'_{ORG,Ox(g)})$ .  $k'_{ORG,Ox(g)}$  and  $k'_{ORG,Ox(aq)}$  are by  
 252 calculated by multiplying the bimolecular reaction rate constant (Table S16) with the corresponding steady-state concentration of oxidant: [ $\bullet OH(g)$ ] =  $1 \times 10^6$   
 253 molecules cm<sup>-3</sup>, [O<sub>3</sub>(g)] = 30 ppbv =  $7.4 \times 10^{11}$  molecules cm<sup>-3</sup>, [ $\bullet OH(aq)$ ] =  $2 \times 10^{-15}$  M ( includes gas-to-aqueous partitioning; Kaur and Anastasio (2017) and  
 254 this study), [O<sub>3</sub>(aq)] =  $3.3 \times 10^{-10}$  M (based on equilibrium with 30 ppbv O<sub>3</sub>(g) and  $K_H = 1.1 \times 10^{-2}$  M atm<sup>-1</sup>; Seinfeld and Pandis (2012)), [<sup>1</sup>O<sub>2</sub>\*(aq)] =  $2 \times 10^{-13}$  M  
 255 in fog (average in Davis fog; Kaur and Anastasio (2017)), and  $1.5 \times 10^{-10}$  M in PM (estimate in PM after accounting for evaporative loss and loss due to organic  
 256 sinks at higher DOC concentrations; Sect. S5). In case of the triplets, in fog [<sup>3</sup>C\*(aq)] =  $2 \times 10^{-13}$  M (average in Davis fog; Kaur and Anastasio (2018)); in PM  
 257 both the lower- and upper-bound concentrations obtained via extrapolation (Table S15) are considered, i.e., [<sup>3</sup>C\*(aq)] =  $1.7 \times 10^{-13}$  M and  $1.5 \times 10^{-10}$  M,  
 258 respectively.

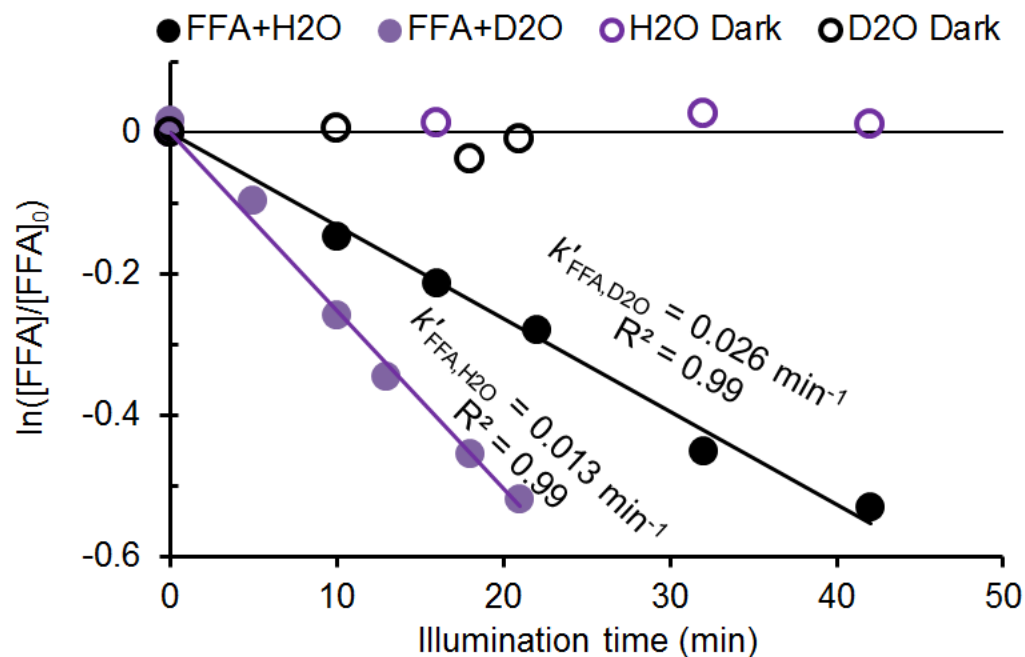
259 <sup>d</sup> Overall lifetime of organic compound, calculated as  $1/k'_{ORG}$ .

260 <sup>e</sup> Percent of organic compound lost due to each pathway, calculated as  $(f_{aq} \times k'_{ORG,Ox(aq)})/k'_{ORG}$  for aqueous pathways and  $((1-f_{aq}) \times k'_{ORG,Ox(g)})/k'_{ORG}$  for gas-phase  
 261 processes. The sum of all pathways for a given compound is sometimes not equal to 100% because of rounding.

262

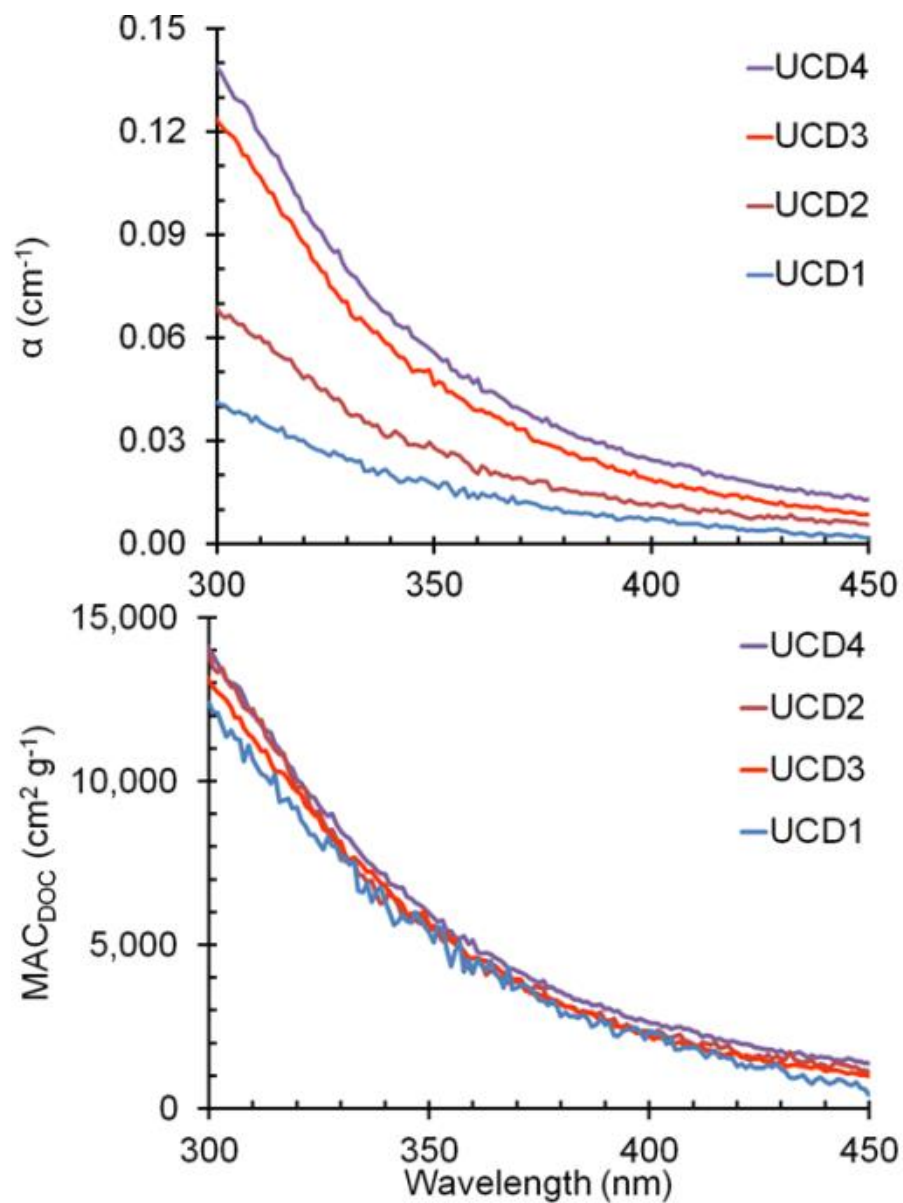


263  
 264 **Figure S1.**  $\cdot\text{OH}$  measurement in extract PME5. Top Panel: Photoformation of phenol in four  
 265 aliquots of the extract spiked with varying benzene concentrations (0.10 to 1.5 mM). The rates of  
 266 phenol formation,  $R_p$ , were determined as the slopes of the linear fits for each of the four data  
 267 sets. Bottom: "Inverse" plot, i.e., the inverse of  $R_p$  vs. the inverse of the benzene concentration.  
 268 The slope and y-intercept from this plot are used to calculate  $P_{\text{OH}}$ ,  $[\cdot\text{OH}]$ , and  $k'_{\text{OH}}$  using  
 269 equations described in Kaur and Anastasio (2017).  $\cdot\text{OH}$  results for all particle extracts are  
 270 tabulated in Table S3.  
 271



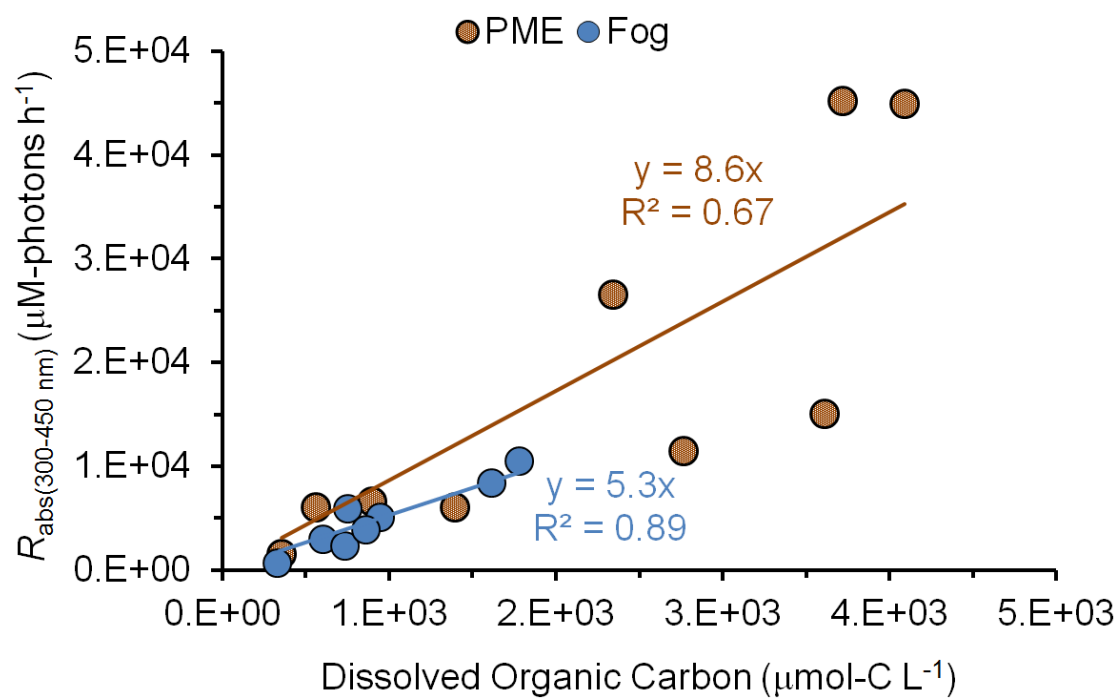
272  
 273 **Figure S2.** Singlet oxygen kinetic measurements in extract PME5 diluted 1:1 (volume:volume)  
 274 with H<sub>2</sub>O or D<sub>2</sub>O. Data show the change in probe concentration (furfuryl alcohol, FFA) with  
 275 illumination time. Closed symbols are illuminated samples while open symbols represent dark  
 276 controls. Equations for calculating <sup>1</sup>O<sub>2</sub>\* steady-state concentrations and rates of photoproduction  
 277 are described in Kaur and Anastasio (2017).





279

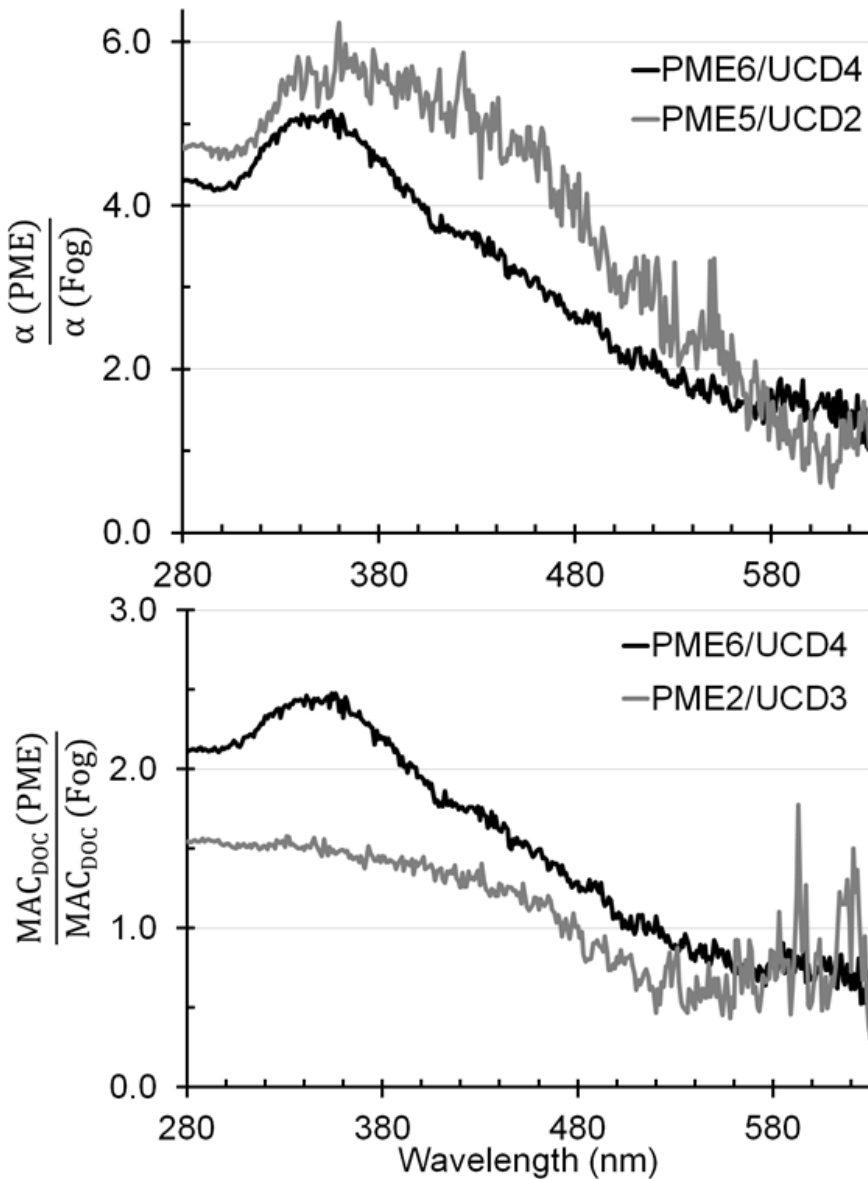
280 **Figure S3.** Top panel: Light absorbance by fog samples collected during 2011-12 in Davis, CA.  
281 The legend shows the sample identities, arranged from the highest absorbing (top) to lowest  
282 absorbing (bottom) at 300 nm. Bottom panel: Mass absorption coefficient of DOC in the Davis  
283 fog samples. All data from Kaur and Anastasio (2017).



284

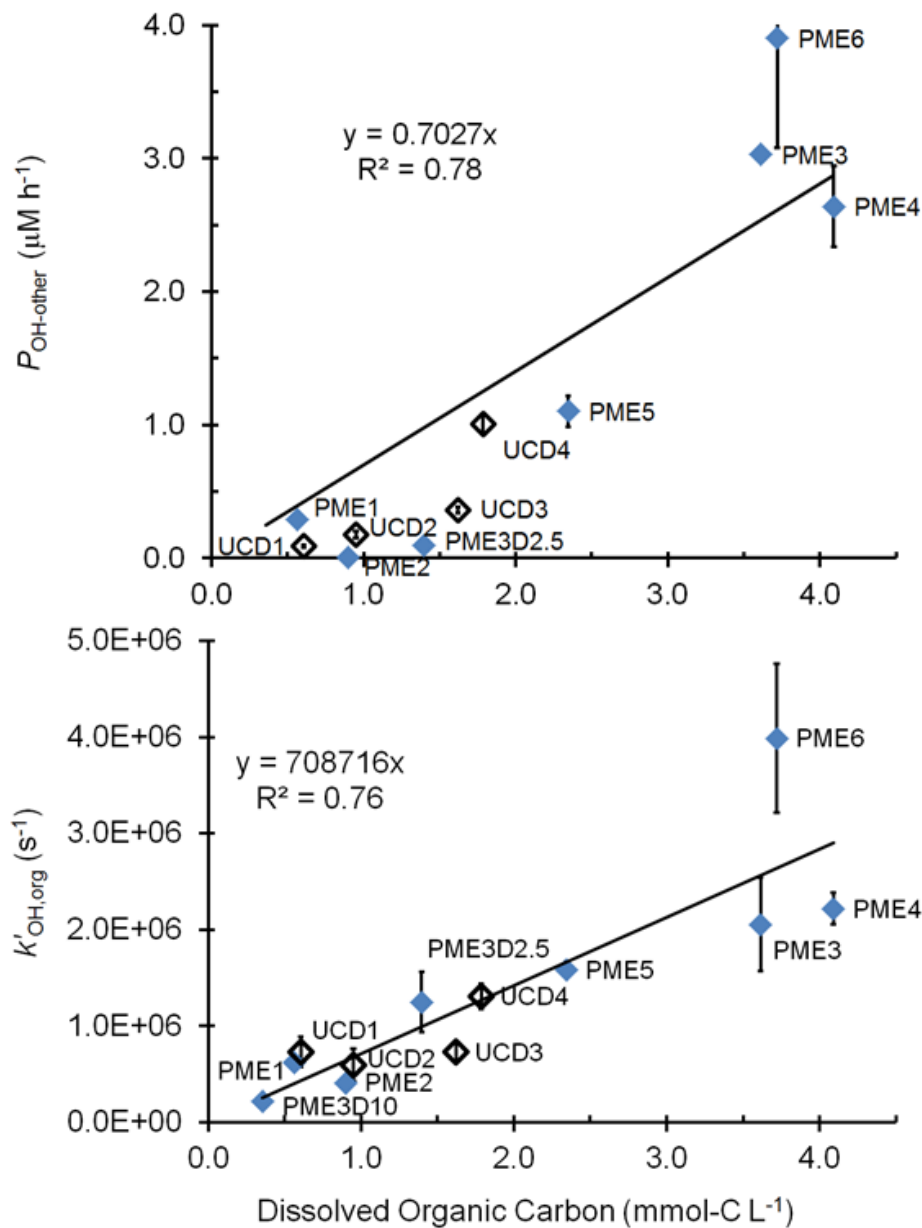
285 **Figure S4.** Correlation between the rate of sunlight absorption ( $R_{\text{abs}}$ ) in the 300-450 nm  
 286 wavelength range and dissolved organic carbon (DOC) for the fog samples (data from Kaur and  
 287 Anastasio (2017)) and particle extracts (PME) (this work). Values for PME in this plot are  
 288 summarized in Table S1.

289



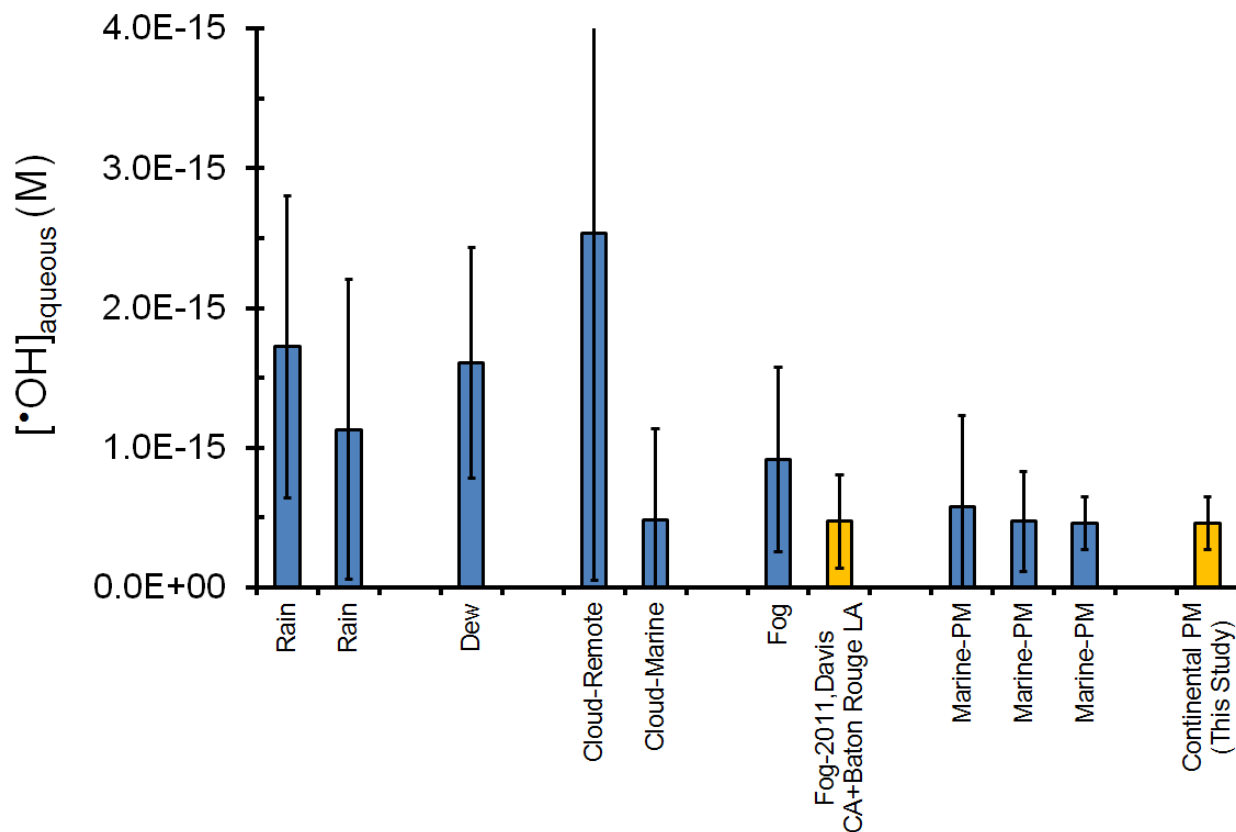
290

291 **Figure S5.** (Top) Ratio of pathlength-normalized absorbance for PME and fog samples with  
 292 highest (black) and median (grey) absorbances. (Bottom): Ratio of mass absorption coefficients  
 293 of DOC in PME and fog samples with highest (black) and median (grey) absorbances.



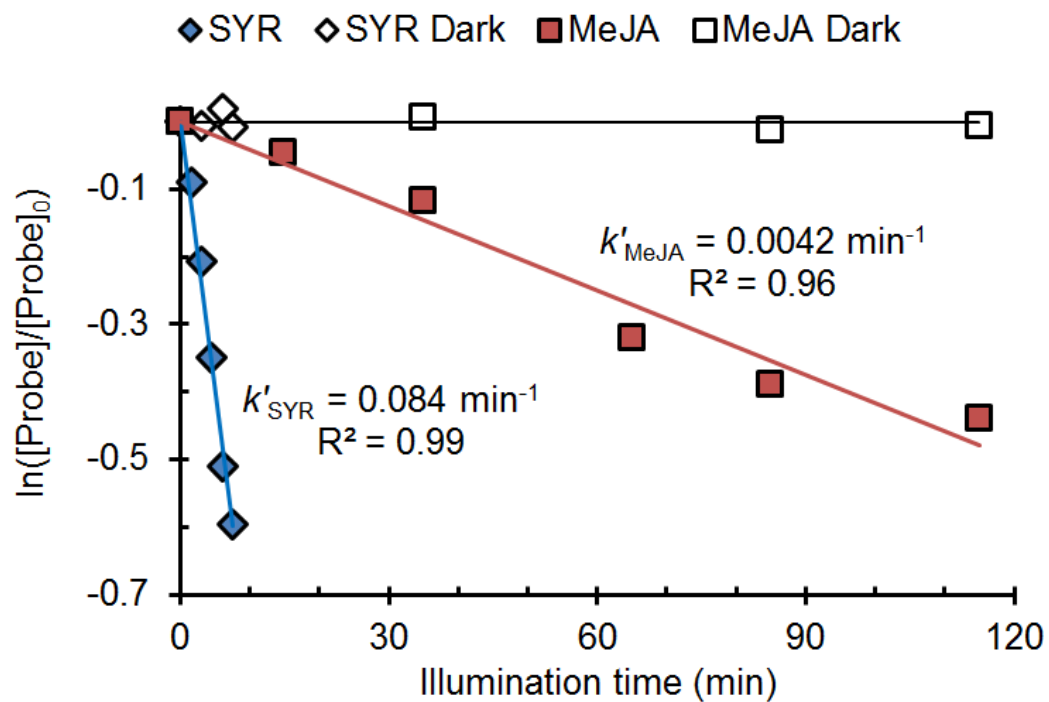
294  
 295 **Figure S6.** (Top) Correlation between the rate of  $\cdot\text{OH}$  photoproduction due to sources other than  
 296 nitrite and nitrate and the concentration of dissolved organic carbon (DOC). While the  $R^2$  value  
 297 for this correlation is relatively high, this is largely driven by the highest three points: most of the  
 298 data are poorly fit by the regression line. (Bottom) Correlation between apparent pseudo-first  
 299 order rate constant for loss of  $\cdot\text{OH}$  due to organic sinks (obtained by subtracting inorganic  
 300 contributions from the measured  $k'_{\text{OH}}$ ) and DOC. Data include measurements in particle extracts  
 301 (measured in this work) and in Davis fogs (Kaur and Anastasio, 2017).

302

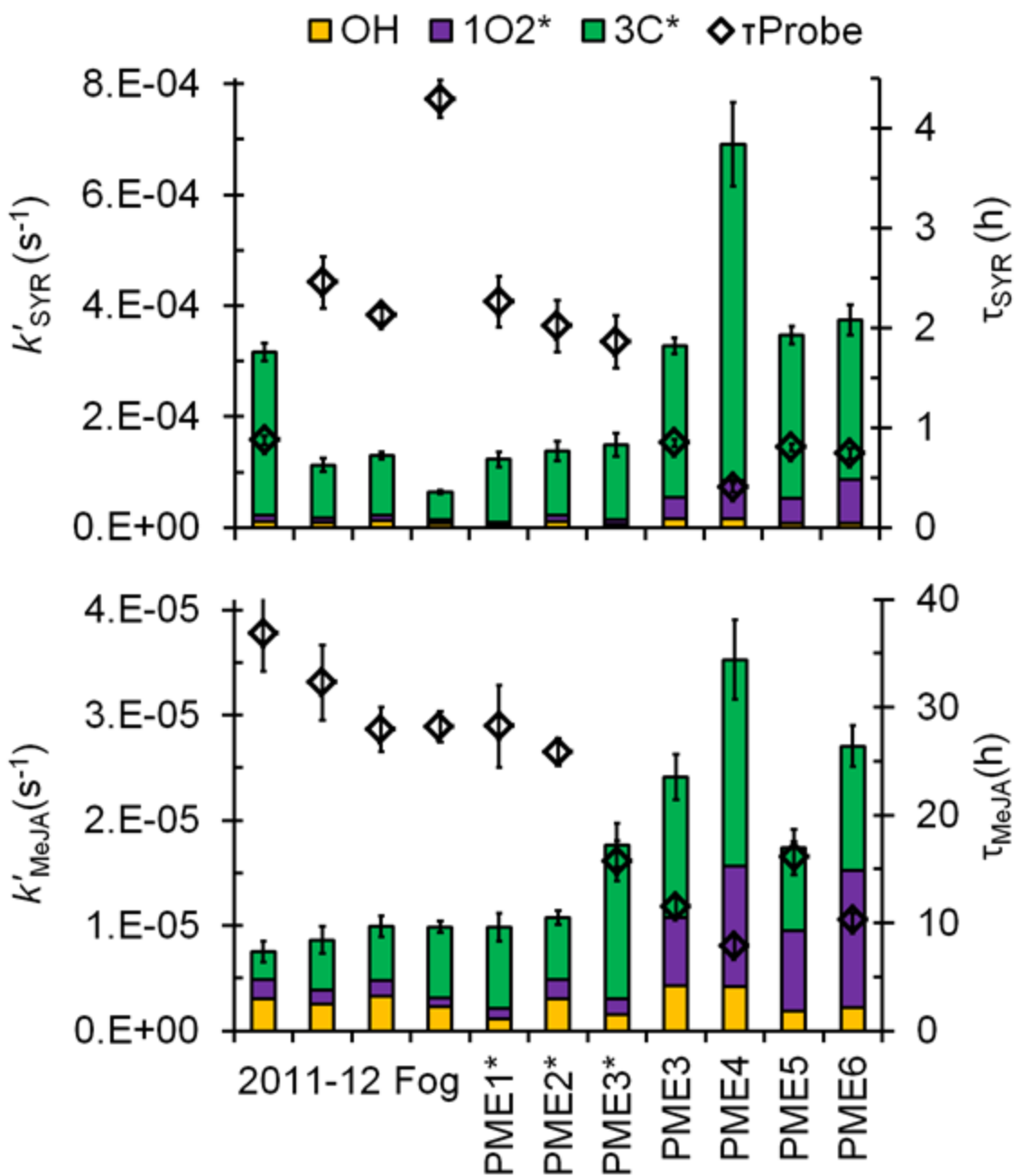


303

304 **Figure S7.** Comparison of hydroxyl radical steady-state concentrations formed *in situ* (i.e., not  
 305 including mass transport of •OH from the gas phase) measured in various atmospheric waters, as  
 306 summarized in Arakaki et al. (2013) (blue bars) and including (in yellow bars) our recent data for  
 307 fog (Kaur and Anastasio, 2017) and current data for PM. Error bars are  $\pm 1\sigma$ , calculated from the  
 308 variability in values used to calculate the mean for a given study.



309  
 310 **Figure S8.** Loss of probes for measuring triplet excited states: syringol (SYR) and methyl  
 311 jasmonate (MeJA) in extract PME5. Closed symbols are illuminated samples while open  
 312 symbols represent dark controls.

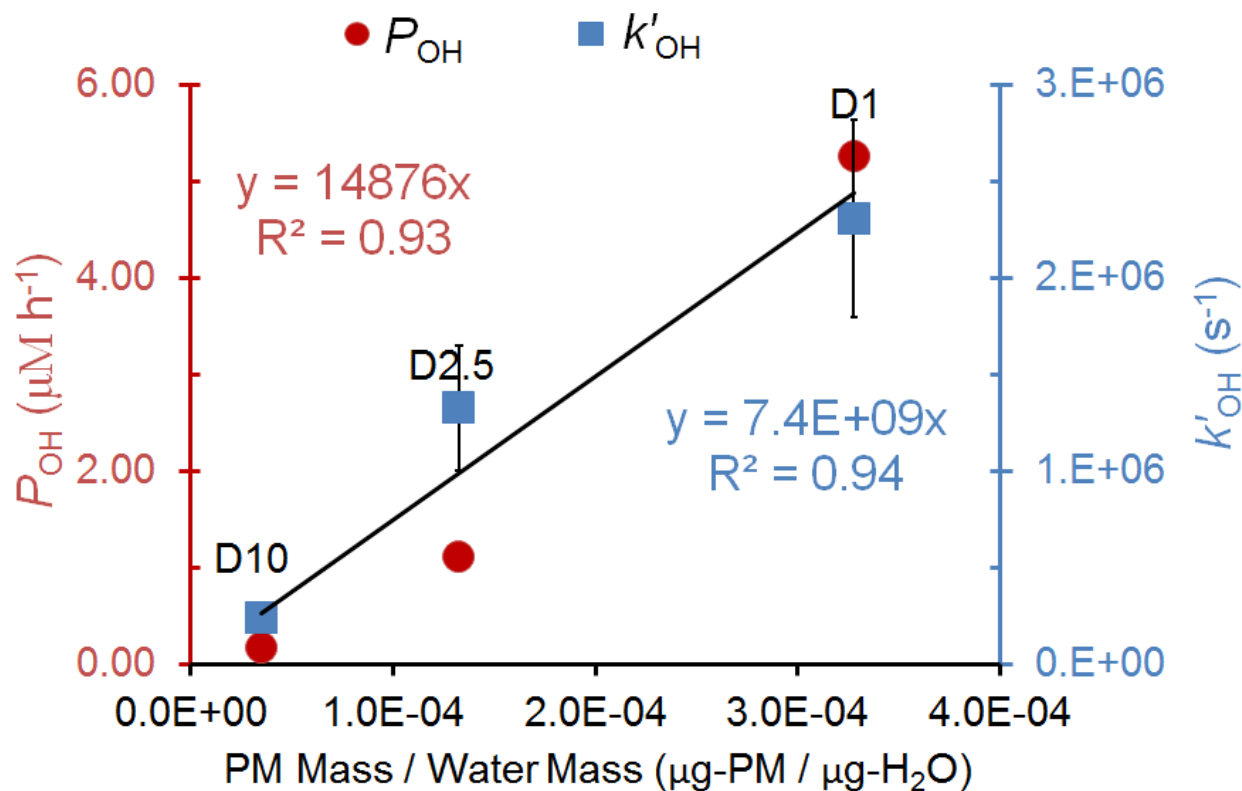


313

314 **Figure S9.** Winter-solstice-normalized pseudo-first-order rate constants ( $k'_{\text{Probe}}$ ) for loss of  
 315 syringol (top panel) and methyl jasmonate (bottom panel). The bar representing each rate  
 316 constant is colored to represent the contributions of hydroxyl radical (yellow), singlet molecular  
 317 oxygen (purple) and triplet excited states (green) to probe loss. The Davis winter-solstice lifetime  
 318 of each probe ( $\tau_{\text{Probe}}$ , black diamonds) is shown on the right y-axis. The first four bars represent  
 319 probe data from wintertime fog waters collected in Davis (Kaur and Anastasio, 2018)

320

321

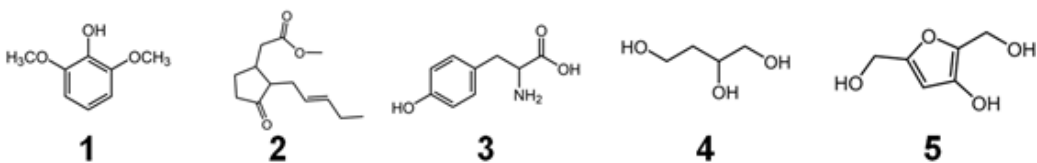


322

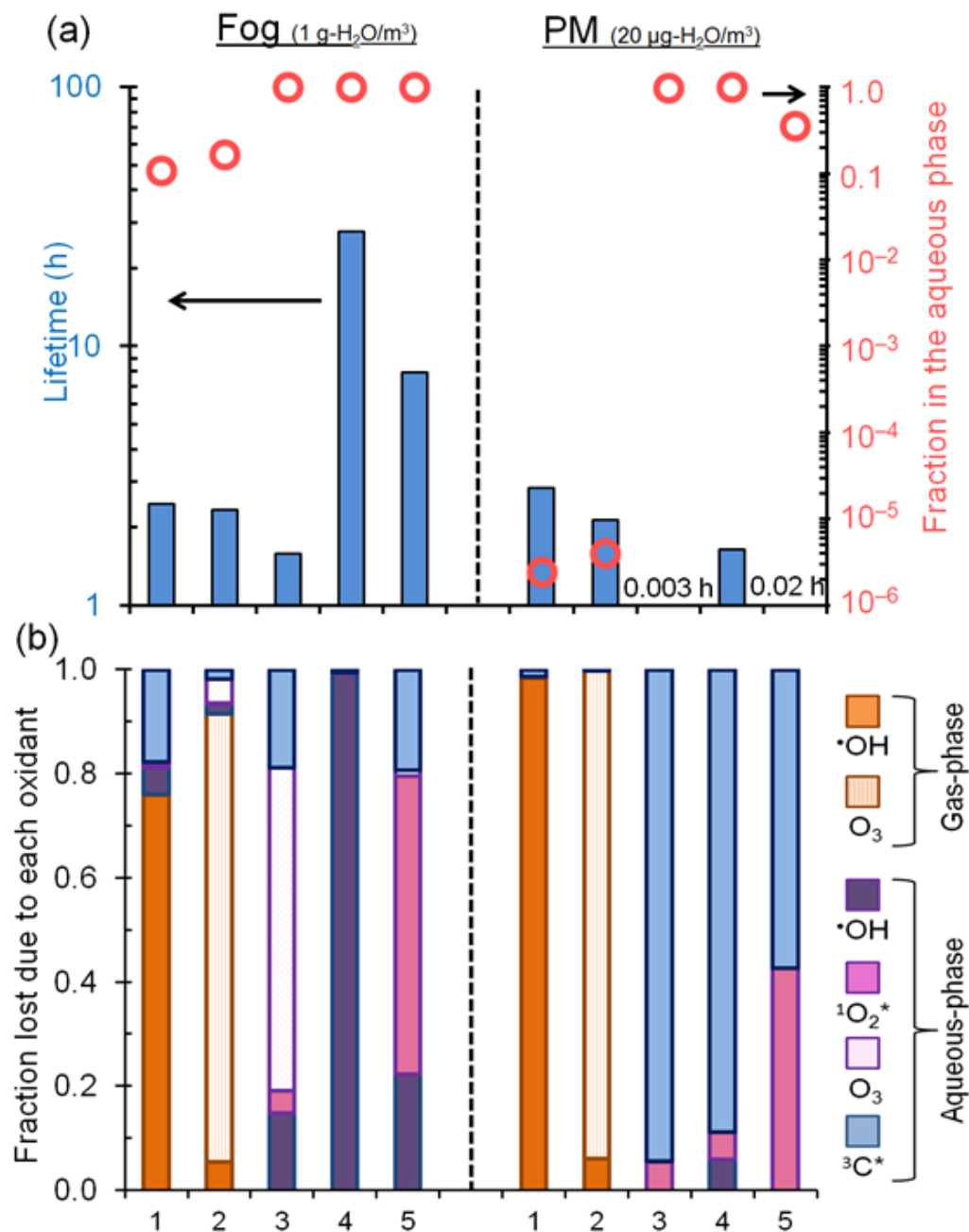
323 **Figure S10.** Dependence of rate of  $\cdot\text{OH}$  photoproduction ( $P_{\text{OH}}$ ; red, left y-axis) and rate constant  
 324 for loss of  $\cdot\text{OH}$  due to natural sinks ( $k'_{\text{OH}}$ ; blue, right y-axis) with PM mass/water mass ratio in  
 325 three PME3D samples. ( $\cdot\text{OH}$  kinetic measurements were not made in the other two PME3D  
 326 samples.) Measurements of  $\cdot\text{OH}$  kinetics in the PME3D samples are discussed in Section S1 and  
 327 shown in Table S3. Using the slopes of the linear relationships (lines overlap but both slopes are  
 328 given) shown here to extrapolate  $P_{\text{OH}}$  and  $k'_{\text{OH}}$  to values under ambient particle conditions ( $1 \mu\text{g-}$   
 329  $\text{PM}/\mu\text{g-H}_2\text{O}$ ) gives  $P_{\text{OH}} = 4.1 \times 10^{-6} \text{ M s}^{-1}$  and  $k'_{\text{OH}} = 7.4 \times 10^9 \text{ s}^{-1}$ . Error bars represent  $\pm 1$   
 330 standard errors and are too small to be visible for  $P_{\text{OH}}$ .

331





$(5.0 \times 10^3)$        $(8.1 \times 10^3)$        $(8.0 \times 10^{10})$        $(4.7 \times 10^{11})$        $(1.1 \times 10^9)$



332

333 **Figure S11.** Fate of five model organic compounds – syringol, methyl jasmonate,  
 334 1,2,4-butanetriol and 3-hydroxy-2,5-bis(hydroxymethyl)furan – under fog (left of vertical dashed  
 335 line) and PM (right of dashed line) conditions using an upper-bound estimate for triplet

336 concentrations in PM. Estimated Henry's law constants for the compounds (in units of  $\text{M atm}^{-1}$ )  
337 are in parentheses beneath each structure. Panel (a): the blue columns represent overall lifetimes  
338 of the organics via both gas and aqueous-phase loss processes, and the red open circles represent  
339 the fractions present in fog or aqueous PM. (b) Fraction of each compound lost via each  
340 pathway. The aqueous triplet concentration in PM is  $1.5 \times 10^{-10}$  M (Table S15, Fig. 5, main text).  
341 All oxidant concentrations and rate constant data are shown in Tables S16 and S17.

## 342 Section S1: Hydroxyl radical measurements in PME3 and PME3D extracts

### 343 S1.1: Determining $\cdot\text{OH}$ steady-state concentrations ( $[\cdot\text{OH}]$ )

344 Typically, for  $\cdot\text{OH}$  measurements we used benzene as the probe. Since benzene is volatile, we  
345 performed the illumination in 5 mL sealed quartz cuvettes (instead of quartz tubes) fully filled  
346 with extract, only withdrawing 100  $\mu\text{L}$  for analysis at each time point to minimize loss of  
347 benzene due to volatilization into the headspace. However, for the PME3D extracts, where we  
348 had limited sample volume, we could not fully fill the 5 mL cuvettes. Due to this limitation, for  
349 the PME3D samples we monitored the loss of 2-methyl-3-buten-2-ol (MBO) to determine  $\cdot\text{OH}$   
350 concentrations, then separately measured the production rate of  $\cdot\text{OH}$  using benzene (for the three  
351 dilutions with sufficient volume), and combined these two measures to determine the  $\cdot\text{OH}$  sink.

352  
353 There are three main reasons we chose MBO as a probe: 1) it is less volatile than benzene in  
354 water, 2) its rate constants with the major photooxidants (i.e.  $\cdot\text{OH}$ ,  $^1\text{O}_2^*$  and  $^3\text{C}_i^*$ ) are known, and  
355 3) its reaction with  $\cdot\text{OH}$  is much faster than with  $^1\text{O}_2^*$  and  $^3\text{C}_i^*$  (see below). Fresh MBO stock  
356 was made one day prior to each experiment. 1.0 mL of acidified (pH 4.2) PME3D extract was  
357 spiked to 75  $\mu\text{M}$  MBO, capped and illuminated with simulated sunlight in a quartz tube of 4 mm  
358 pathlength. Throughout the illumination period, MBO loss was measured with HPLC-UV (eluent  
359 of 20% acetonitrile: 80% Milli-Q water, flow rate of 0.6 mL/min, detection wavelength of 200  
360 nm and column temperature of 35°C). The pseudo-first-order rate constant for loss of MBO  
361 ( $k'_{\text{MBO}}$ ;  $\text{s}^{-1}$ ) was obtained as the negative of the slope of the plot of  $\ln([\text{MBO}]/[\text{MBO}]_0)$  versus  
362 time then normalized to Davis-winter-solstice light using an analog of Eq. (4) in the main text.  
363 Because MBO is not a specific probe for  $\cdot\text{OH}$ , its loss in each sample is the sum of all its loss  
364 pathways:

$$365 \quad k'_{\text{MBO}} = k_{\text{MBO}+\text{OH}} [\cdot\text{OH}] + k_{\text{MBO}+^1\text{O}_2^*} [^1\text{O}_2^*] + \Sigma(k_{\text{MBO}+^3\text{C}_i^*} [^3\text{C}_i^*]) + j_{\text{MBO}} \quad (\text{S1})$$

366 where  $[\cdot\text{OH}]$ ,  $[^1\text{O}_2^*]$  and  $\Sigma[^3\text{C}_i^*]$  are the steady-state concentrations of the photooxidants. The  
367 variables  $k_{\text{MBO}+\text{OH}}$  ( $7.4 (\pm 0.5) \times 10^9 \text{ M}^{-1} \text{ s}^{-1}$ ; (Richards-Henderson et al., 2014c)),  $k_{\text{MBO}+^1\text{O}_2^*}$  ( $7.0$   
368  $(\pm 1.0) \times 10^5 \text{ M}^{-1} \text{ s}^{-1}$ ; (Richards-Henderson et al., 2014c)) and  $k_{\text{MBO}+^3\text{C}_i^*}$  (discussed below) are the  
369 second-order rate constants for reactions of MBO.  $j_{\text{MBO}}$  is the rate constant for direct  
370 photodegradation of the probe and is negligible for our illumination times ( $2.7 \times 10^{-7} \text{ s}^{-1}$ ).

371

372 Eq. (S1) has two unknown quantities: 1) [ $\cdot\text{OH}$ ] and 2) the loss of MBO due to triplets, i.e.,  
 373  $\Sigma(k_{\text{MBO}+3\text{Ci}^*}[\text{}^3\text{C}_i^*])$ . To get [ $\cdot\text{OH}$ ], we first estimated MBO loss due to triplets ( $\Sigma(k_{\text{MBO}+3\text{Ci}^*}[\text{}^3\text{C}_i^*])$ )  
 374 by using two assumptions about the triplets. Our first assumption is that all loss of the triplet  
 375 probe syringol is due to  $\text{}^3\text{C}^*$  and  $\text{}^1\text{O}_2^*$ , i.e.,  $\cdot\text{OH}$  is a negligible oxidant for SYR, based on our  
 376 measurements in the other samples, PME1-6, where the fraction of SYR lost due to  $\text{}^3\text{C}^*$  and  $\text{}^1\text{O}_2^*$   
 377 (combined) is 91 to 98% (Table S8).

378  
 379 The loss of syringol in the PME3D extracts is the sum of its loss due to  $\cdot\text{OH}$ ,  $\text{}^1\text{O}_2^*$  and  $\text{}^3\text{C}^*$ :

$$381 \quad k'_{\text{SYR}} = k_{\text{SYR}+\text{OH}} [\cdot\text{OH}] + k_{\text{SYR}+1\text{O}_2^*} [\text{}^1\text{O}_2^*] + \Sigma(k_{\text{SYR}+3\text{C}_i^*} [\text{}^3\text{C}_i^*]) \quad (\text{S2})$$

382  
 383 Direct photodegradation of syringol is negligible, and the contributions of other oxidants have  
 384 been previously determined to be small (Section 2.5.3, main text). Based on our first assumption,  
 385  $k_{\text{SYR}+\text{OH}} [\cdot\text{OH}]$  is much smaller than the sum of the other two terms on the right-hand side of Eq.  
 386 (S2) and this equation can be simplified to:

$$388 \quad k'_{\text{SYR}} \approx k_{\text{SYR}+1\text{O}_2^*} [\text{}^1\text{O}_2^*] + \Sigma(k_{\text{SYR}+3\text{C}_i^*} [\text{}^3\text{C}_i^*]) \quad (\text{S3})$$

389  
 390 Our second assumption is that the reactivity of the triplet mixture in the PM extracts most closely  
 391 resembles a binary mixture of the model triplets  $\text{}^3\text{MAP}^*$  and  $\text{}^3\text{DMB}^*$ — since these are the best  
 392 triplet matches obtained for majority of the particle extracts (Table S11). For simplicity, we use a  
 393 1:1 mixture of the two model triplets. Thus, for  $k_{\text{SYR}+3\text{C}_i^*}$  we used a triplet-syringol rate constant  
 394 ( $\pm \sigma$ ) of  $3.7 (\pm 0.2) \times 10^9 \text{ M}^{-1} \text{ s}^{-1}$ , which is the average of  $k_{\text{SYR}+3\text{MAP}^*}$  and  $k_{\text{SYR}+3\text{DMB}^*}$  (Table S10)  
 395 in Eq. (S3) to obtain the triplet steady-state concentration:

$$397 \quad \Sigma[\text{}^3\text{C}_i^*] = \frac{k'_{\text{SYR}} - (k_{\text{SYR}+1\text{O}_2^*} [\text{}^1\text{O}_2^*])}{k_{\text{SYR}+3\text{C}_i^*}} \quad (\text{S4})$$

398  
 399 Using the measured singlet oxygen concentration, [ $\text{}^1\text{O}_2^*$ ], for each PME3 dilution we determine  
 400  $\Sigma[\text{}^3\text{C}_i^*]$  in Eq. (S4), which we then plug into Eq. (S1), along with  $k_{\text{MBO}+3\text{C}_i^*} = 3.4 (\pm 0.4) \times 10^7 \text{ M}^{-1}$

401  $s^{-1}$ , the average of  $k_{\text{MBO}+33\text{MAP}^*}$  and  $k_{\text{MBO}+3\text{DMB}^*}$  (Richards-Henderson et al. (2014c)) to obtain  
 402 the first iteration of  $[\cdot\text{OH}]$ :

403

$$404 \quad [\cdot\text{OH}] = \frac{k'_{\text{MBO}} - k_{\text{MBO}+1\text{O}_2^*}[\cdot\text{O}_2^*] - \Sigma(k_{\text{MBO}+3\text{C}_i^*}[\cdot\text{C}_i^*])}{k_{\text{MBO}+3\text{C}_i^*}} \quad (\text{S5})$$

405

406 We then remove the first assumption and plug these  $[\cdot\text{OH}]$  values into Eq. (S2) to get a second  
 407 set of  $\Sigma[\cdot\text{C}_i^*]$  values, which we use in Eq. (S1) to obtain the second iteration of  $[\cdot\text{OH}]$ . We  
 408 continue this iterative process until the  $[\cdot\text{OH}]$  values change by less than 0.01% (Table S18). The  
 409 fourth iteration values were corrected for light screening (discussed in Sect. 2.5.1 of the main  
 410 text) and are shown in Table S3.

411 **Table S18.** Hydroxyl radical steady-state concentrations in four iterations

Sample ID	Hydroxyl Radical Steady-State Concentration				
	$(10^{-16}) \text{ M}$				
	$[\cdot\text{OH}]$ Iteration 1	$[\cdot\text{OH}]$ Iteration 2	$[\cdot\text{OH}]$ Iteration 3	$[\cdot\text{OH}]$ Iteration 4	$\Delta[\cdot\text{OH}]^a$
PME3D0.5	5.54 (1.87)	5.72 (1.93)	5.73 (1.93)	5.73 (1.39)	0.0034%
PME3D1	5.74 (1.91)	5.93 (1.97)	5.94 (1.97)	5.94 (1.40)	0.0034%
PME3D1.3	2.23 (0.76)	2.31 (0.77)	2.31 (0.79)	2.31 (0.57)	0.0034%
PME3D2.5*	2.19 (0.75)	2.26 (0.77)	2.26 (0.77)	2.26 (0.57)	0.0034%
PME3D10	1.89 (0.68)	1.95 (0.70)	1.95 (0.70)	1.95 (0.54)	0.0034%

412 Uncertainties in parentheses are  $\pm 1$  standard error.

413 <sup>a</sup> Difference in the third and fourth iteration  $[\cdot\text{OH}]$  values.

414

### 415 **S1.2: Rate of $\cdot\text{OH}$ photoproduction ( $P_{\text{OH}}$ )**

416 Similar to the other extracts, in the PME3 samples we used benzene as the probe measure  $\cdot\text{OH}$   
 417 photoformation (Kaur and Anastasio, 2017; Anastasio and McGregor, 2001; Zhou and Mopper,  
 418 1990). A 5.0 mL aliquot of extract was acidified to pH 4.2 ( $\pm 0.2$ ) and spiked with 1500  $\mu\text{M}$   
 419 benzene, which should scavenge essentially all  $\cdot\text{OH}$ . The solution was illuminated in a capped,

420 sealed quartz cuvette with a 1 cm pathlength (Sect. 2.5.1 in main text). In all cases, phenol  
421 concentration increased linearly with time, and the rate of phenol formation ( $R_p$ ) was obtained as  
422 the slope of the plot of phenol concentration versus time. We then plotted  $1/R_p$  versus  
423  $1/[\text{Benzene}]$  and the intercept of that plot gave the experimentally measured rate of  $\cdot\text{OH}$   
424 photoproduction ( $P_{\text{OH,EXP}}$ ) (Zhou and Mopper, 1990). Measured rates of  $\cdot\text{OH}$  formation were  
425 normalized to the rate expected under midday Davis, CA winter-solstice sunlight ( $P_{\text{OH}}$ ) based on  
426 2-nitrobenzaldehyde (2NB) actinometry:

$$427 \quad P_{\text{OH}} = P_{\text{OH,EXP}} \times \frac{j_{2\text{NB,WIN}}}{j_{2\text{NB,EXP}}} \quad (\text{S6})$$

428 where  $j_{2\text{NB,WIN}}$  is the rate constant for loss of 2NB measured at midday near the winter solstice in  
429 Davis ( $0.0070 \text{ s}^{-1}$ ; Anastasio and McGregor, (2001)), and  $j_{2\text{NB,EXP}}$  is the measured rate constant  
430 for loss of 2NB on the day of the experiment. Due to the volume requirements of this technique,  
431 we were only able to measure  $P_{\text{OH}}$  in three extracts – PME3, PME3D2.5\* and PME3D10.

432

### 433 **S1.3 Rate constant for loss of $\cdot\text{OH}$ due to natural sinks ( $k'_{\text{OH}}$ )**

434 In the PME3 samples we calculated the pseudo-first-order rate constant for loss of  $\cdot\text{OH}$  due to  
435 natural sinks by dividing the measured rate of  $\cdot\text{OH}$  photoproduction determined with benzene  
436 (Sect. S1.2) by the measured  $\cdot\text{OH}$  steady-state concentration determined with MBO (Sect. S1.1):

$$437 \quad k'_{\text{OH}} = \frac{P_{\text{OH}}}{[\cdot\text{OH}]} \quad (\text{S7})$$

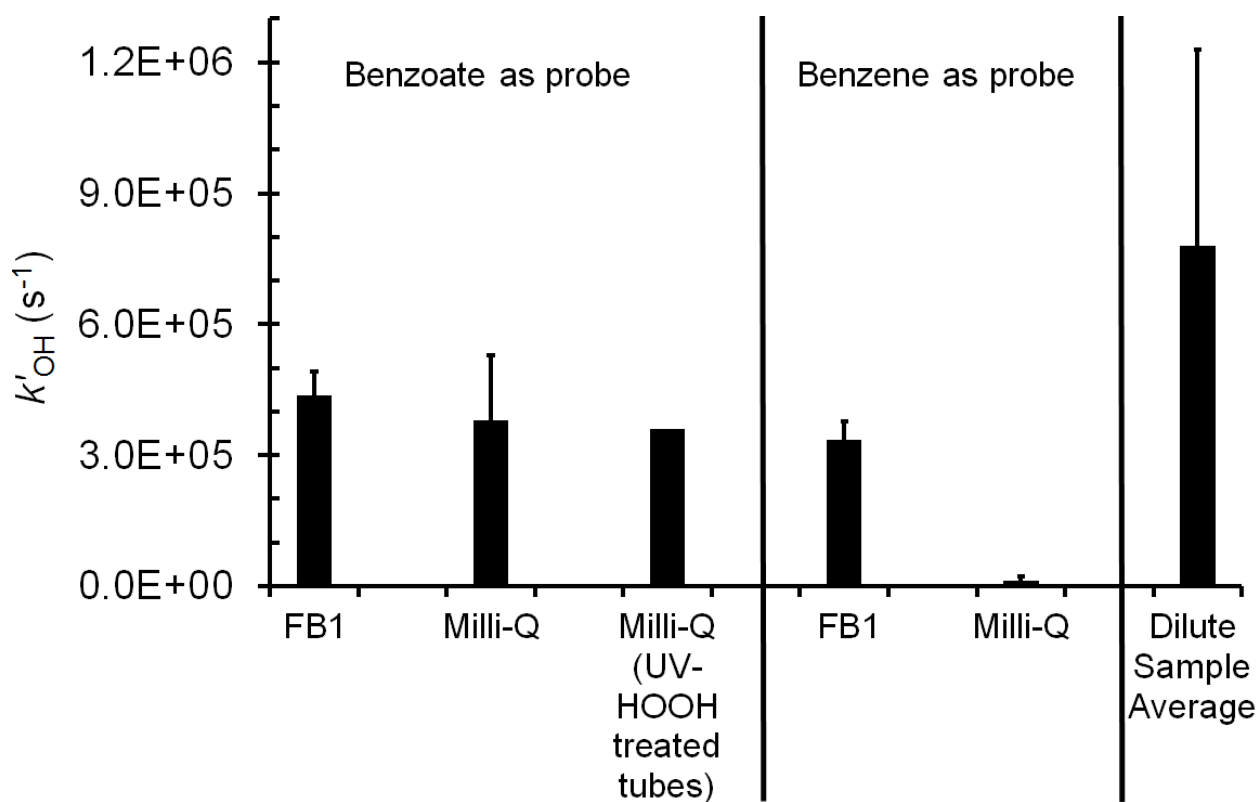
## 438 Section S2: $\cdot\text{OH}$ sink measurements ( $k'_{\text{OH}}$ ) in field blanks FB1 and FB2

439 We also measured the rate constant for loss of  $\cdot\text{OH}$  due to natural sinks ( $k'_{\text{OH}}$ ) in field blank FB1,  
440 which was extracted under the “dilute conditions”, i.e. each  $2 \times 2$  cm filter square was extracted  
441 in 2.5 mL Milli-Q.

442  
443 In the early stages of this project, we used benzoate as an  $\cdot\text{OH}$  probe (Anastasio and McGregor,  
444 2001), which reacts with  $\cdot\text{OH}$  to form m-hydroxybenzoic acid, m-HBA (and other products),  
445 which was quantified using UV-HPLC. Four 5.0 mL aliquots of extract were spiked with 100–  
446 1500  $\mu\text{M}$  of sodium benzoate/benzoic acid solution (20 mM) at pH 4.2. Since  $P_{\text{OH}}$  in FB1 was  
447 below our detection limit (Table S3), we added 200  $\mu\text{M}$  hydrogen peroxide as an  $\cdot\text{OH}$  source to  
448 each aliquot in order to measure the  $\cdot\text{OH}$  sinks. Aliquots were illuminated in capped quartz tubes  
449 with a 0.4 cm pathlength (Sect. 2.3 main text). The formation of m-HBA was linear in all cases,  
450 and the slope of the plot of [m-HBA] versus time in each aliquot is the rate of m-HBA formation  
451 ( $R_{\text{P}}$ ,  $\mu\text{M min}^{-1}$ ). Similar to the benzene technique, we then plotted  $1/R_{\text{P}}$  versus  $1/[\text{benzoate}]$ , used  
452 the slope and y-intercept of the inverse plot to obtain  $P_{\text{OH}}$ ,  $k'_{\text{OH}}$  and  $[\cdot\text{OH}]$ , which were  
453 normalized to Davis midday solstice sunlight conditions.  $k'_{\text{OH}}$  measured using benzoate was 4.4  
454 ( $\pm 0.5$ )  $\times 10^5 \text{ s}^{-1}$ , and represented 56% of the dilute sample average (PME1\*, PME2\*,  
455 PME3D2.5). Because this is high, we ran a number of tests to identify the source of the  
456 background  $\cdot\text{OH}$  sinks in FB1, starting with measuring  $k'_{\text{OH}}$  in two Milli-Q solutions containing  
457 only HOOH and probe stocks to identify whether these were the source of contamination.  $k'_{\text{OH}}$  in  
458 Milli-Q was nearly as high as in FB1: even after rigorously cleaning the quartz tubes using a  
459 UV+HOOH treatment (Chen et al., 2016),  $k'_{\text{OH}}$  was not lowered appreciably (Fig. S12). Since at  
460 this point, it appeared that the probe chemicals (sodium benzoate and benzoic acid) could be  
461 contaminated, we decided to switch to benzene as the  $\cdot\text{OH}$  probe.

462  
463 The experimental procedure for the benzene technique is very similar to the benzoate technique,  
464 except that the aliquots of FB1 were acidified to pH 4.2 ( $\pm 0.2$ ) using 10 mM sulfuric acid. While  
465 the  $k'_{\text{OH}}$  value using benzene was slightly lower than the benzoate case (3.4 ( $\pm 0.4$ )  $\times 10^5 \text{ s}^{-1}$ ), it  
466 still represented 43% of the PM sample average. We then performed the benzene technique in  
467 Milli-Q water: the resulting  $k'_{\text{OH}}$  of 1.2 ( $\pm 0.1$ )  $\times 10^4 \text{ s}^{-1}$  was more than 10 times lower than the  
468 other measurements, typical of solutions without any background organic contamination (Chen

469 et al., 2016). This was the lowest  $k'_{OH}$  measured in our trials so, we chose to proceed with  
470 benzene as the probe for measuring  $\cdot OH$  in the particle extracts.



471  
472 **Figure S12.** Measured pseudo-first-order rate constant for loss of  $\cdot OH$  due to natural sinks ( $k'_{OH}$ )  
473 in various solutions using sodium benzoate/benzoic acid and benzene as  $\cdot OH$  probes. Samples  
474 labeled “Milli-Q” contain only probe and HOOH. Samples labeled “FB1” are measurements in  
475 the extract solution of Field Blank 1. “Dilute Sample Average” is the average of the  $k'_{OH}$   
476 measurements in PME1\*, PME2\* and PME3D2.5\* (Table S3).

477  
478 We next determined  $k'_{OH}$  in FB2 with benzene under standard extract conditions (1 mL Milli-Q  
479 per filter square). However, the resulting value of  $2.7 (\pm 0.1) \times 10^5 s^{-1}$  is not much lower than the  
480 value in (more dilute) FB1 determined with benzoate and is 20 times higher than the Milli-Q  
481 value. But because the  $k'_{OH}$  value in the standard extracts (PME3D1-PME6) is high (Table S3),  
482 the corresponding FB2 value is only 11% of the standard sample average. One plausible  
483 contributing factor to the high  $k'_{OH}$  in the field blanks is that organic matter is coming off the  
484 filter material during extraction; we see this in the DOC measurements for both field blanks  
485 (Table S2). For future studies, we recommend first evaluating a few different types of particle



486 filters by making background  $k'_{OH}$  measurements and then picking the filters that introduce the  
487 least contamination.

488

489 We did not adjust values of  $k'_{OH}$  measured in the particle extracts for the field blank rate  
490 constants. If we had adjusted them,  $\bullet OH$  concentrations would have increased by 50% in the  
491 “dilute” extracts and by 10% in the standard extracts. However, the concentrations would still be  
492 similar to fog. Additionally, this adjustment would have no effect on the extrapolation to ambient  
493 PM conditions, since  $[\bullet OH]$  in all PME3D extracts would go up equally.

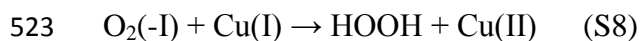
### 494 **Section S3: Other oxidants in PM extracts**

495 Since the probes we use for triplet determination do not react with only triplets (Eq. (5), main  
496 text), we account for the contributions of  $^1\text{O}_2^*$  and  $^{\bullet}\text{OH}$  to probe loss. However, it is also  
497 possible that other oxidants (that we do not measure) are also contributing to triplet probe loss.  
498 Here we examine this possibility for triplet probe loss in the PM extracts. In our previous  
499 measurements of photooxidants in fog water (Kaur and Anastasio, 2018), we estimated the  
500 importance of hydroperoxyl radical/superoxide radical anion ( $\text{HO}_2^{\bullet}/^{\bullet}\text{O}_2^-$ ), ozone ( $\text{O}_3$ ), carbonate  
501 radical ( $^{\bullet}\text{CO}_3^-$ ) and hydrogen ion/hydrated electron ( $\text{H}^{\bullet}(\text{aq})/\text{e}^-(\text{aq})$ ) and found that these species  
502 in total contributed less than 7 % to the average measured syringol loss. To do this calculation  
503 for our PM extracts, we estimate the steady-state concentrations of these oxidants in the  
504 illuminated extracts and, using reaction rate constants available in literature, calculate a pseudo-  
505 first-order rate constant for their reaction with syringol. We then compare that to the average ( $\pm$   
506  $\sigma$ ) measured syringol loss in the standard extracts,  $k'_{\text{SYR}} = 3.9 (\pm 1.3) \times 10^{-4} \text{ s}^{-1}$ . As we noted in  
507 our previous paper, there are insufficient rate constants in the literature for reactions of methyl  
508 jasmonate in order to estimate its potential loss to other oxidants.

#### 509 **Hydroperoxyl Radical / Superoxide Radical Anion ( $\text{O}_2(-\text{I})$ )**

510 Hydroperoxyl radical and superoxide radical anion (i.e.,  $\text{O}_2(-\text{I})$ ) are a conjugate acid-base pair;  
511 the  $\text{p}K_{\text{a}}$  of  $\text{HO}_2^{\bullet}$  is  $4.75 \pm 0.08$  (Bielski et al., 1985). Since the pH of our extracts was adjusted to  
512 ambient particle pH of 4.2 (Parworth et al., 2017), the mole fractions of  $\text{HO}_2^{\bullet}$  and  $^{\bullet}\text{O}_2^-$  in the  
513 extracts are 0.78 and 0.22, respectively. There are no rate constants available for reaction of  
514 either species with syringol (2,6-dimethoxyphenol) so we use the fastest reported rate constants  
515 for reactions of similar compounds with  $^{\bullet}\text{O}_2^-$  and  $\text{HO}_2^{\bullet}$ . For substituted phenols, the rate  
516 constant for reaction of  $^{\bullet}\text{O}_2^-$  with guaiacol (2-methoxyphenol) is  $2.5 \times 10^3 \text{ M}^{-1} \text{ s}^{-1}$  (Yasuhisa et  
517 al., 1993); for  $\text{HO}_2^{\bullet}$ , the rate constant with catechol (1,2-benzenediol) is  $4.7 \times 10^4 \text{ M}^{-1} \text{ s}^{-1}$   
518 (Bielski, 1983). At pH 4.2, the mole-fraction weighted rate constant, used as the proxy for  
519  $k_{\text{SYR}+\text{O}_2(-\text{I})}$ , is  $3.7 \times 10^4 \text{ M}^{-1} \text{ s}^{-1}$ .

520 To estimate  $\text{O}_2(-\text{I})$  concentrations in the extracts, we use previously measured rates of HOOH  
521 formation in illuminated fog waters from California's Central Valley since these two oxidants  
522 are intimately connected (Deguillaume et al., 2004; Anastasio, 1994):



524 The maximum measured production rate of HOOH,  $P_{HOOH}$ , in illuminated Central Valley fogs is  
525  $3 \mu M h^{-1}$  ( $8.3 \times 10^{-10} M s^{-1}$ ; Anastasio (1994)). We expect that  $P_{HOOH}$  in particle extracts will be  
526 higher than fog, so we use an enhancement factor based on the observed increase in singlet  
527 oxygen concentrations in the standard extracts, which is a factor of seven higher than Davis fog  
528 average (Table S7). The reaction rate constants for  $\cdot O_2^-$  and  $HO_2\cdot$  reacting with Cu(I) are  $9.4 \times$   
529  $10^9 M^{-1} s^{-1}$  (Piechowski et al., 1993) and  $3.5 \times 10^9 M^{-1} s^{-1}$  (Berdnikov, 1973), respectively,  
530 which gives an overall, mole-fraction-weighted reaction rate constant,  $k_{O_2(-I)+Cu(I)}$ , of  $4.8 \times 10^9 M^{-1}$   
531  $s^{-1}$ . We assume that the Cu(I) concentration is similar to that of  $O_2(-I)$  (e.g.,  $[Cu(I)] \approx 1$  nM in  
532 the daytime urban cloud scenario of Deguillaume et al. (2004)). Solving the rate equation for S8  
533 with these inputs gives an  $O_2(-I)$  steady-state concentration of  $1.1 \times 10^{-9} M$ . At this  
534 concentration, the estimated loss rate constant for syringol due to  $O_2(-I)$ ,  $k'_{SYR,O_2(-I)}$  is  $4.1 \times 10^{-5}$   
535  $s^{-1}$ , which would account for 11 % of the average observed syringol loss. This suggests that  
536 superoxide is a minor sink for syringol in our samples, although it does appear to be more  
537 significant in particle extracts than fog.

### 538 **Ozone ( $O_3$ )**

539 Based on the Henry's law constant for ozone at 25°C ( $K_H = 1.1 \times 10^{-2} M atm^{-1}$  (Seinfeld and  
540 Pandis, 2012) and assuming a gas-phase mixing ratio for  $O_3$  of 30 ppbv, gives an initial aqueous-  
541 phase concentration of ozone in our samples of  $3.3 \times 10^{-10} M$ . The actual concentration is likely  
542 lower since our samples are capped during illumination. The bimolecular rate constant for  
543 reaction of ozone with syringol is not available in the literature, so we estimate the rate constant  
544 by using the value for phenol ( $k_{PhOH+O_3} = 1.3 \times 10^3 M^{-1} s^{-1}$ ) (Hoigné and Bader, 1983) with an  
545 enhancement factor of 10 based on the measured ratio of phenol and syringol rate constants for  
546 reaction with  $^3DMB^*$  (Smith et al., 2015). Under these assumptions, ozone is a very minor sink  
547 for syringol in the fog samples ( $k'_{SYR,O_3} = 4.3 \times 10^{-6} s^{-1}$ ), accounting for 1% of the average  
548 measured syringol loss.

### 549 **Carbonate Radical ( $\cdot CO_3^-$ )**

550 The carbonate radical is formed mainly from the reactions of bicarbonate ( $HCO_3^-$ ) and carbonate  
551 ( $CO_3^{2-}$ ) ions with  $\cdot OH$  and triplet CDOM species. Although DOM components are likely

552 important sinks for  $\bullet\text{CO}_3^-$ , this quenching is poorly understood (Canonica et al., 2005; Vione et  
553 al., 2014; Huang and Mabury, 2000). There are no published measurements of  $\bullet\text{CO}_3^-$  in  
554 atmospheric waters, so we use the typical steady-state concentration measured in surface waters  
555 of  $2 \times 10^{-14}$  M determined using N,N-dimethylaniline as a probe (Huang and Mabury, 2000;  
556 Zeng and Arnold, 2012). There are concerns that aniline probes overestimate  $\bullet\text{CO}_3^-$  since they  
557 also react rapidly with triplets (Rosario-Ortiz and Canonica, 2016), so we treat this as an upper-  
558 bound estimate. We do not apply an enhancement factor in this case since DOM appears to play  
559 the dual role of source and sink. While  $\bullet\text{CO}_3^-$  reacts rapidly with electron-rich phenolates (i.e., a  
560 deprotonated phenol), at pH 4.2 syringol is in the neutral, less reactive form. There are no rate  
561 constants available for  $\bullet\text{CO}_3^-$  reacting with methoxyphenols, so we assume the value with SYR  
562 is 10 times higher than that with phenol ( $4.9 \times 10^6 \text{ M}^{-1}\text{s}^{-1}$ ; Chen et al. (1975)). This results in a  
563 pseudo-first-order rate constant for loss of SYR due to carbonate radical of  $1 \times 10^{-6} \text{ s}^{-1}$ , which  
564 represents a negligible 0.3% of the average measured syringol loss rate constant in our standard  
565 PM extracts.

#### 566 **Hydrogen Ion / Aquated Electron ( $\text{H}^\bullet_{(\text{aq})}/\text{e}^-_{(\text{aq})}$ )**

567 Hydrogen ion ( $\text{H}^\bullet$ ) and aquated electron ( $\text{e}^-_{(\text{aq})}$ ) can be formed during irradiation or illumination  
568 of dissolved organic matter in natural waters; these exist as a conjugate acid-base pair with a  $\text{p}K_a$   
569 of 9.6 (Kozmér et al., 2014; Buxton et al., 1988a). In our extracts at pH 4.2, the predominant  
570 species would be  $\text{H}^\bullet_{(\text{aq})}$ . Zepp et al. (1987) determined an average steady-state concentration of  
571  $\text{e}^-_{(\text{aq})}$  in sunlight-illuminated lake waters to be  $1.2 \times 10^{-17}$  M. Similar to  $^1\text{O}_2^*$ , since DOM is the  
572 main source of  $\text{e}^-_{(\text{aq})}$ , we assume an enhancement factor of seven in the steady-state  
573 concentration of  $\text{e}^-_{(\text{aq})}$ . As an upper bound, we assume the  $\text{H}^\bullet$  concentration to be equal to this.  
574 The rate constant for syringol reacting with  $\text{H}^\bullet$  is not known. Using the average rate constant for  
575 methoxyphenol,  $2.1 \times 10^9 \text{ M}^{-1}\text{s}^{-1}$  (O'Neill et al., 1975; Neta and Schuler, 1972), the pseudo-  
576 first-order rate constant for loss of SYR due to hydrogen ion is  $1.7 \times 10^{-7} \text{ s}^{-1}$ , which would  
577 account for only 0.04% of the average observed syringol loss.

#### 578 **Combined Contributions from Other Oxidants**

579 Based on our upper-bound estimates, the total rate constant for loss of syringol due to  $\text{HO}_2^\bullet/\text{O}_2^-$ ,  
580  $\text{O}_3$ ,  $\bullet\text{CO}_3^-$  and  $\text{H}^\bullet_{(\text{aq})}/\text{e}^-_{(\text{aq})}$  is  $\sim 4.6 \times 10^{-5} \text{ s}^{-1}$ , which is only 12% of the average measured

581 syringol loss rate constant. Since this is small, our assumption that the loss of syringol is mainly  
582 due to  $\cdot\text{OH}$ ,  $^1\text{O}_2^*$  and  $^3\text{C}^*$ (Eq. (6), main text) seems valid.

583  
584  
585  
586  
587  
588  
589  
590  
591  
592  
593  
594  
595  
596  
597  
598  
599  
600  
601  
602  
603  
604  
605  
606  
607  
608  
609  
610  
611  
612  
613

#### Section S4: Impacts of mass transport and increasing organic concentration on estimates of aqueous photooxidant concentrations in ambient particles

The steady-state concentration of an oxidant reflects the balance between its rate of formation ( $P_{OX}$ ) and first-order rate constant for loss ( $k'_{OX} = 1 / \tau_{OX}$ ):

$$[OX] = P_{OX} / k'_{OX} \quad (S9)$$

where  $k'_{OX}$  is the sum of all the pseudo-first-order sinks of the oxidant, In Figure 5 we extrapolate the aqueous concentrations of  $^1O_2^*$ ,  $^3C^*$ , and  $\cdot OH$  from our relatively dilute measurements to the approximately 1000-times more concentrated conditions of ambient particles. However, the extrapolations in the figure do not consider interaction with the gas phase or a potential change in the sinks as the solutions get more concentrated. Here we consider these factors to refine our estimates of oxidant concentrations under particle conditions. We roughly estimate the gas-phase influence using a simplified case with an aqueous particle radius ( $R_p$ ) of 0.5  $\mu m$ , temperature of 298 K, and total pressure of 1 atm.

In the case of hydroxyl radical, based on our measurements and previous work (Arakaki et al., 2013; Anastasio and Newberg, 2007), the concentrations of the major aqueous sources (nitrate, nitrite, and unknown species) and sinks (organic compounds) both scale linearly with PM aqueous mass concentration, indicating that  $[\cdot OH]$  should be independent of dilution. However, this does not consider the influence of the gas phase. The extremely short lifetime of  $\cdot OH$  in the particles ( $1/k'_{OH} \sim 1 \times 10^{-10}$  s) indicates that this oxidant will not be at Henry's law equilibrium and that the gas phase will be a source of  $\cdot OH$ . We estimate the rate of this gas-phase mass transport to the particles ( $P_{MT}$ ) using the Fuchs-Sutugin transition regime formula (Seinfeld and Pandis, 2012) with an estimated gas-phase  $\cdot OH$  concentration of  $1 \times 10^6$  molecules  $cm^{-3}$  and a mass accommodation coefficient of 1. Under these conditions the rate of  $\cdot OH$  gas-to-particle transport is  $1.4 \times 10^{-6} M s^{-1}$ , approximately a third of the extrapolated production rate from our measured rates of aqueous photochemistry ( $P_{OH}$ ). If we consider both the aqueous- and gas-phase sources of  $\cdot OH$  to the particles, we estimate a steady-state concentration of

614  $[\cdot\text{OH}(\text{aq})] = (P_{\text{OH}} + P_{\text{MT}})/k'_{\text{OH}} = 1 \times 10^{-15} \text{ M}$  (S10)

615  
616 In the case of singlet molecular oxygen, there is little gas-phase data, but past estimates  
617 suggested concentrations on the order of  $1 \times 10^8$  molecules  $\text{cm}^{-3}$  (Demerjian, 1974). At Henry's  
618 law equilibrium, this gas-phase concentration corresponds to an aqueous concentration of  $5 \times 10^{-14}$   
619 M (using the Henry's law constant for ground state  $\text{O}_2$ ,  $1.3 \times 10^{-3} \text{ M atm}^{-1}$  at 298 K; Seinfeld  
620 and Pandis (2012)). Since this estimated aqueous concentration is many orders of magnitude  
621 lower than our extrapolated particle concentration, the net effect of mass transport will be to  
622 move  $^1\text{O}_2^*$  from the particles to the gas phase. The slow step in this evaporation of  $^1\text{O}_2^*$  is  
623 liquid-phase diffusion, which has a characteristic time of

624  
625  $\tau_{\text{LD}} = R_p^2/(\pi^2 \times D_{\text{aq}})$  (S11)

626  
627 where  $D_{\text{aq}}$  is the aqueous diffusion coefficient, approximately  $1 \times 10^{-5} \text{ cm}^2 \text{ s}^{-1}$  if we assume an  
628 aqueous particle. Solving this equation for our simplified particle case gives a characteristic time  
629 of  $6 \times 10^{-6} \text{ s}$ . The inverse of this is the approximate first-order rate constant for liquid-phase  
630 diffusion, i.e.,  $k'_{\text{LD}} \sim 2 \times 10^5 \text{ s}^{-1}$ ; thus evaporation is a significant sink since this is roughly equal  
631 to the first-order rate constant for deactivation of  $^1\text{O}_2^*$  in water ( $k'_{\text{H}_2\text{O}} = 2.2 \times 10^5 \text{ s}^{-1}$ ; Bilski et al.  
632 (1997)).

633  
634 Under cloud and fog drop conditions (and in our PM extracts) this deactivation by water is the  
635 major sink for singlet oxygen, but under the more concentrated conditions of aqueous particles,  
636 organic compounds might also be important. To very roughly estimate this organic sink, we  
637 multiply our average DOC concentration in PM extracts (3.4 mM-C; Table S2) by a factor of  
638 1000 to extrapolate to ambient PM conditions and assume all of this material is soluble, resulting  
639 in an aqueous concentration of particulate organics of 3.4M-C. If each organic molecule has an  
640 average of 6 C atoms (i.e., the average is the same as levoglucosan), this corresponds to a water-  
641 soluble organic concentration of 0.56 M. We apportion this total concentration based on the  
642 emissions measurements of Jen et al. (2018), where water-soluble organics in biomass burning  
643 emissions are roughly 50% sugars, 25% phenols, and 25% organic nitrogen. Table S19 below  
644 shows the resulting estimated particle concentrations, along with an estimated average rate  
645 constant for each class based on the compilation by Wilkinson et al. (1995). Summing the

646 contributions from each compound class we estimate a total pseudo-first order rate constant for  
647 loss of  $^1\text{O}_2^*$  by soluble organics in the particles of  $2.8 \times 10^6 \text{ s}^{-1}$ .

648

649 **Table S19.** Estimates of the organic sink of  $^1\text{O}_2^*$  in aqueous particles

Compound Class	Dissolved Concentration (M)	2 <sup>nd</sup> -order Rate Constant Range ( $\text{M}^{-1} \text{ s}^{-1}$ )	Assumed 2 <sup>nd</sup> -order $k$ ( $\text{M}^{-1} \text{ s}^{-1}$ )	$k'_{\text{ORG}}$ ( $\text{s}^{-1}$ )
Sugars	0.28	$10^4$	$10^4$	2800
Phenols	0.14	$10^6 - 10^7$	$10^7$	$1.4 \times 10^6$
Organic Nitrogen	0.14	$10^3 - 10^9$	$10^7$	$1.4 \times 10^6$

650

651 The resulting estimate for the steady-state concentration of  $^1\text{O}_2^*$  in the particles is

652

653 
$$[^1\text{O}_2^*] = P_{1\text{O}_2^*} / (k'_{\text{H}_2\text{O}} + k'_{\text{LD}} + k'_{\text{ORG}}) = (5.0 \times 10^{-4} \text{ M s}^{-1}) / (3.2 \times 10^6 \text{ s}^{-1}) \quad (\text{S12})$$

654

655 where the numerator, i.e., the rate of  $^1\text{O}_2^*$  photoformation in PM is obtained by extrapolating the  
656 measured rate in the PME3D samples. This gives an adjusted  $[^1\text{O}_2^*]$  value of  $1.5 \times 10^{-10} \text{ M}$ ,  
657 which is 14 times lower than that extrapolated from the aqueous data in Figure 5 (and Table S15)  
658 because of the organic and evaporative sinks. Based on the terms in the denominator of Eq.  
659 (S12), our simple estimate predicts that roughly 90% of  $^1\text{O}_2^*$  in the particle water is lost via  
660 reaction with phenols and organic nitrogen.

661

662 Finally, for the case of triplet excited states we expect that (to a first approximation) mass  
663 transport will have no significant impact on the particle concentration. Since most of the BrC  
664 precursors for  $^3\text{C}^*$  are likely in the particle phase (rather than the gas phase) we expect that gas-  
665 phase concentrations of triplets are relatively small and that the gas phase is not a significant  
666 source of triplets to the particles. We also expect that evaporation of triplets is minor since their  
667 lifetimes are relatively short (1  $\mu\text{s}$  based just on  $\text{O}_2$  as a sink) and their gas-particle partitioning  
668 (like that of their BrC precursors) is strongly tilted toward the particle phase. Thus we assume  
669 that the particle concentration of triplets is relatively unaffected by mass transport. As for  
670 potential organic sinks of  $^3\text{C}^*$ , the curvature shown in Figures 4 and 5 is likely due to organics



671 becoming major sinks in the more concentrated PM extracts; this is accounted for in our  
672 hyperbolic fit. However, it is also possible that the curvature is noise and that the  ${}^3\text{C}^*$   
673 concentration in particles is much higher than extrapolated using the hyperbolic fit in Figure 5;  
674 we explore both of these scenarios in the main text.

675

### 676 **Section S5: Estimating triplet characteristics in particle extract PME3**

677 We can use our measurements of triplet steady-state concentrations in the PME3 dilution series  
678 to derive the pseudo-first-order rate constant for triplet formation and the overall rate constant for  
679 triplet reaction and quenching by DOC.

680 The rate of triplet formation ( $P_{3\text{C}^*}$ ) from the photoexcitation of chromophores ‘C’ in the extracts  
681 can be expressed as:

682

$$683 \quad P_{3\text{C}^*} = j_{\text{abs}} \times \Phi_{\text{ISC}} \times [\text{C}] \quad (\text{S13})$$

684

685 where  $j_{\text{abs}}$  is the rate constant for light absorption ( $\text{s}^{-1}$ ) by C and  $\Phi_{\text{ISC}}$  is the intersystem crossing  
686 quantum yield, i.e., the fraction of the first excited single state,  $\text{S}_1$ , that forms the lowest triplet  
687 excited state,  $\text{T}_1$ . Assuming the chromophore concentration is a fraction  $f$  (mole-chromophore  
688 mole- $\text{C}^{-1}$ ) of the DOC concentration (mole- $\text{C L}^{-1}$ ), the rate of triplet formation can be expressed  
689 as

690

$$691 \quad P_{3\text{C}^*} = j_{\text{abs}} \times \Phi_{\text{ISC}} \times f \times [\text{DOC}] \quad (\text{S14})$$

692

693 The rate constant for loss of the triplet ( $k'_{3\text{C}^*}$ ;  $\text{s}^{-1}$ ) in an extract is the sum of all its loss pathways:

694

$$695 \quad k'_{3\text{C}^*} = k_{3\text{C}^*+\text{O}_2} [\text{O}_2] + k_{\text{rxn}} [\text{DOC}] + k_{\text{Q}} [\text{DOC}] \quad (\text{S15})$$

696

697 where  $k_{3\text{C}^*+\text{O}_2}$  is the bimolecular rate constant for  $\text{O}_2$  quenching (we use the average value for the  
698 three model triplets with measurements,  $2.8 (\pm 0.4) \times 10^9 \text{ M}^{-1}\text{s}^{-1}$ ; Table S11);  $[\text{O}_2]$  is the  
699 dissolved oxygen concentration ( $284 \mu\text{M}$  at  $20 \text{ }^\circ\text{C}$ ) (USGS, 2018);  $k_{\text{rxn}}$  ( $\text{M}^{-1}\text{s}^{-1}$ ) is the rate  
700 constant for reaction of triplet with dissolved organics; and  $k_{\text{Q}}$  ( $\text{M}^{-1}\text{s}^{-1}$ ) is the rate constant for  
701 the non-reactive quenching of triplet by DOC (Smith et al., 2014).

702 Assuming steady state, the triplet concentration is the ratio of its rate of photoproduction and its  
 703 rate constant for loss:

$$704 \quad [{}^3\text{C}^*] = \frac{P_3\text{C}^*}{k'_{3\text{C}^*}} = \frac{j_{\text{abs}} \times \Phi_{\text{ISC}} \times f \times [\text{DOC}]}{k_{3\text{C}^*+O_2} [\text{O}_2] + (k_{\text{rxn}} + k_{\text{Q}}) [\text{DOC}]} \quad (\text{S16})$$

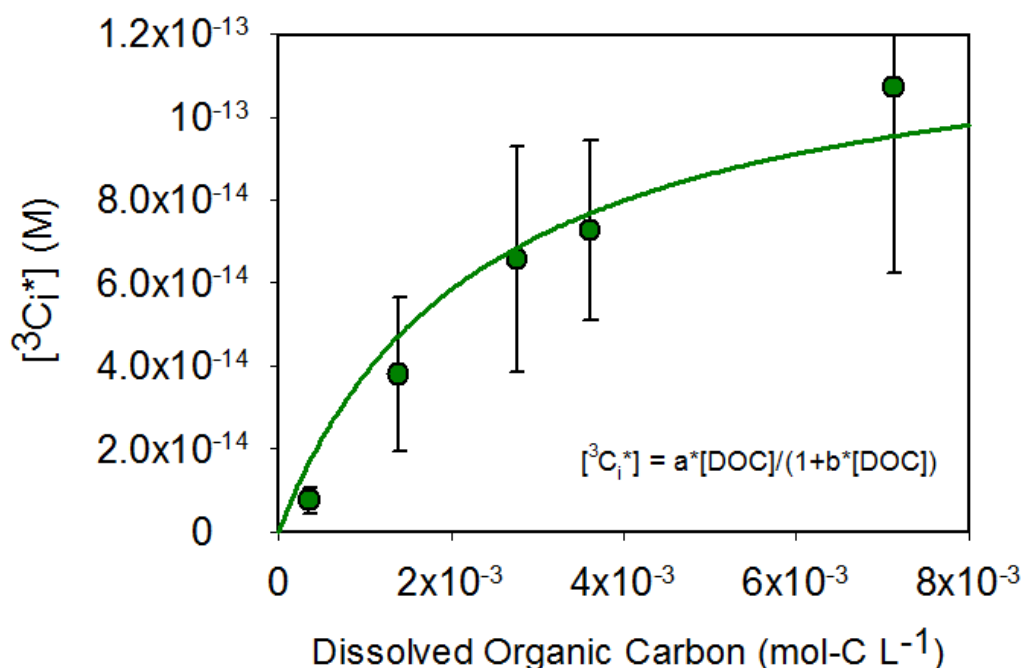
705 This can be re-written as

$$706 \quad [{}^3\text{C}^*] = \frac{\left(\frac{j_{\text{abs}} \times \Phi_{\text{ISC}} \times f}{k_{3\text{C}^*+O_2} [\text{O}_2]}\right) \times [\text{DOC}]}{1 + \left(\frac{k_{\text{rxn}} + k_{\text{Q}}}{k_{3\text{C}^*+O_2} [\text{O}_2]}\right) \times [\text{DOC}]} \quad (\text{S17})$$

707 We then fit our triplet steady-state concentration measurements in the PME3D extracts to the  
 708 following two-parameter equation:

$$709 \quad [{}^3\text{C}^*] = \frac{a [\text{DOC}]}{1 + b [\text{DOC}]} \quad (\text{S18})$$

710 The regression fit is shown in Fig. S13 and the parameters for the fit obtained using Sigmaplot  
 711 12.0 are:  $a = 5.4 \times 10^{-11}$  and  $b = 425 \text{ M}^{-1}$ . Using these parameters, we calculate that the rate  
 712 constant for triplet formation, i.e.,  $j_{\text{abs}} \times \Phi_{\text{ISC}} \times f$ , is  $4.3 (\pm 0.7) \times 10^{-5} \text{ s}^{-1}$  and the sum of the  
 713 reaction and quenching rate constants for the triplets by DOC, i.e.,  $k_{\text{rxn}} + k_{\text{Q}}$ , is  $3.4 (\pm 0.5) \times 10^8 \text{ L}$   
 714  $\text{mol-C}^{-1} \text{ s}^{-1}$ .



715  
 716 **Figure S13.** Change in triplet steady-state concentration with dissolved organic carbon  
 717 concentration in the PME3D extracts. Error bars represent  $\pm 1$  standard error in measured triplet  
 718 concentrations (Table S13). Regression line was obtained by fitting the experimental data to the  
 719 form of the equation shown in the figure (modified hyperbola I). Parameters for the fit were

720 obtained using Sigmaplot 12.0 ( $a = 5.4 \times 10^{-11}$  and  $b = 425 \text{ M}^{-1}$ ). The DOC value for sample  
721 PME3D0.5 (which had very limited volume) is estimated based on results for the other four  
722 dilutions and given in Table S2.

723 **References**

- 724 Anastasio, C.: Aqueous phase photochemical formation of hydrogen peroxide in authentic  
725 atmospheric waters and model compound solutions, Ph.D. Dissertation, Duke University,  
726 1994.
- 727 Anastasio, C., and McGregor, K. G.: Chemistry of fog waters in California's central valley: 1. In  
728 situ photoformation of hydroxyl radical and singlet molecular oxygen, *Atmos. Environ.*,  
729 35, 1079-1089, 2001.
- 730 Anastasio, C., and Newberg, J. T.: Sources and sinks of hydroxyl radical in sea-salt particles, *J.*  
731 *Geophys. Res.*, 112, D10306, 2007.
- 732 Anbar, M., Meyerstein, D., and Neta, P.: Reactivity of aliphatic compounds towards hydroxyl  
733 radicals, *Journal of the Chemical Society B: Physical Organic*, 742-747, 1966.
- 734 Andreev, P. Y.: Reaction of ozone with five-membered hetarenes in a liquid phase, *Russ. J.*  
735 *Appl. Chem.*, 85, 1395-1398, 2012.
- 736 Arakaki, T., Anastasio, C., Kuroki, Y., Nakajima, H., Okada, K., Kotani, Y., Handa, D., Azechi,  
737 S., Kimura, T., Tsuchi, A., and Miyagi, Y.: A general scavenging rate constant for  
738 reaction of hydroxyl radical with organic carbon in atmospheric waters, *Environ. Sci.*  
739 *Technol.*, 47, 8196-8203, 2013.
- 740 Atkinson, R., Aschmann, S. M., Fitz, D. R., Winer, A. M., and Pitts, J. N.: Rate constants for the  
741 gas-phase reactions of O<sub>3</sub> with selected organics at 296 K, *Int. J. Chem. Kinet.*, 14, 13-  
742 18, 1982.
- 743 Atkinson, R., Aschmann, S. M., and Carter, W. P.: Kinetics of the reactions of O<sub>3</sub> and OH  
744 radicals with furan and thiophene at 298±2 K, *Int. J. Chem. Kinet.*, 15, 51-61, 1983.
- 745 Atkinson, R., Baulch, D., Cox, R., Crowley, J., Hampson, R., Hynes, R., Jenkin, M., Rossi, M.,  
746 Troe, J., and Subcommittee, I.: Evaluated kinetic and photochemical data for atmospheric  
747 chemistry: Volume II—gas phase reactions of organic species, *Atmos. Chem. Phys.*, 6,  
748 3625-4055, 2006.
- 749 Barker, G., Fowles, P., and Stringer, B.: Pulse radiolytic induced transient electrical conductance  
750 in liquid solutions. Part 2.—radiolysis of aqueous solutions of NO<sub>3</sub><sup>-</sup>, NO<sub>2</sub><sup>-</sup> and Fe(CN)<sub>6</sub><sup>3-</sup>,  
751 *J. Chem. Soc. Faraday Trans.*, 66, 1509-1519, 1970.
- 752 Berdnikov, V.: Catalytic activity of the hydrated copper ion in the decomposition of hydrogen  
753 peroxide, *Russ. J. Phys. Chem.*, 47, 1060-1062, 1973.
- 754 Bertolotti, S. G., García, N. A., and Argüello, G. A.: Effect of the peptide bond on the singlet-  
755 molecular-oxygen-mediated sensitized photo-oxidation of tyrosine and tryptophan  
756 dipeptides. A kinetic study, *Journal of Photochemistry and Photobiology B: Biology*, 10,  
757 57-70, 1991.
- 758 Bielski, B.: Evaluation of the reactivities of HO<sub>2</sub>/O<sub>2</sub> with compounds of biological interest, *Oxy*  
759 *Radicals and Their Scavenger Systems*. G. Cohen and RA Greenwald (Editors), 1, 1-7,  
760 1983.
- 761 Bielski, B. H. J., Cabelli, D. E., Arudi, R. L., and Ross, A. B.: Reactivity of HO<sub>2</sub>/O<sub>2</sub><sup>-</sup> radicals in  
762 aqueous solution, *Journal of Physical and Chemical Reference Data*, 14, 1041-1100,  
763 1985.
- 764 Bilski, P., Holt, R. N., and Chignell, C. F.: Properties of singlet molecular oxygen O<sub>2</sub> (1Δg) in  
765 binary solvent mixtures of different polarity and proticity, *Journal of Photochemistry and*  
766 *Photobiology A: Chemistry*, 109, 243-249, 1997.

767 Buxton, G. V., Greenstock, C. L., Helman, W. P., and Ross, A. B.: Critical review of rate  
768 constants for reactions of hydrated electrons, hydrogen atoms and hydroxyl radicals  
769 ( $\cdot\text{OH}/\text{O}^-$ ) in aqueous solution, *J. Phys. Chem. Ref. Data*, 17, 513-886, 1988a.

770 Buxton, G. V., Wood, N. D., and Dyster, S.: Ionisation Constants of  $\cdot\text{OH}$  And  $\text{HO}_2^-$  in Aqueous  
771 Solution up to 200°C. A Pulse Radiolysis Study, *J. Chem. Soc., Faraday Trans.*, 84,  
772 1113-1121, 1988b.

773 California Air Resources Board, iADAM database: Air Quality Data Statistics:  
774 <https://www.arb.ca.gov/adam>, access: June 6, 2018.

775 Canonica, S., Hellrung, B., and Wirz, J.: Oxidation of phenols by triplet aromatic ketones in  
776 aqueous solution, *J. Phys. Chem. A*, 104, 1226-1232, 2000.

777 Canonica, S., Kohn, T., Mac, M., Real, F. J., Wirz, J., and von Gunten, U.: Photosensitizer  
778 method to determine rate constants for the reaction of carbonate radical with organic  
779 compounds, *Environmental science & technology*, 39, 9182-9188, 2005.

780 Chen, S.-N., Hoffman, M. Z., and Parsons Jr, G. H.: Reactivity of the carbonate radical toward  
781 aromatic compounds in aqueous solution, *J. Phys. Chem.*, 79, 1911-1912, 1975.

782 Chen, Z., Chu, L., Galbavy, E. S., Ram, K., and Anastasio, C.: Hydroxyl radical in/on  
783 illuminated polar snow: Formation rates, lifetimes, and steady-state concentrations,  
784 *Atmos. Chem. Phys.*, 16, 9579-9590, 2016.

785 Deguillaume, L., Leriche, M., Monod, A., and Chaumerliac, N.: The role of transition metal ions  
786 on  $\text{HO}_x$  radicals in clouds: a numerical evaluation of its impact on multiphase chemistry,  
787 *Atmos Chem Phys*, 4, 95-110, 2004.

788 Demerjian, K. L.: The mechanism of photochemical smog formation, *Adv. Environ. Sci.*  
789 *Technol.*, 4, 1-262, 1974.

790 Hess, M., Koepke, P., and Schult, I.: Optical properties of aerosols and clouds: The software  
791 package OPAC, *Bulletin of the American meteorological society*, 79, 831-844, 1998.

792 Hoigné, J., and Bader, H.: Rate constants of reactions of ozone with organic and inorganic  
793 compounds in water—II: Dissociating organic compounds, *Water Res.*, 17, 185-194,  
794 1983.

795 Huang, J., and Mabury, S. A.: Steady-state concentrations of carbonate radicals in field waters,  
796 *Environmental Toxicology and Chemistry*, 19, 2181-2188, 2000.

797 Hunter, T.: Radiationless transition  $T_1 \rightarrow S_0$  in aromatic ketones, *Transactions of the Faraday*  
798 *Society*, 66, 300-309, 1970.

799 Jen, C. N., Hatch, L. E., Selimovic, V., Yokelson, R. J., Weber, R., Fernandez, A. E., Kreisberg,  
800 N. M., Barsanti, K. C., and Goldstein, A. H.: Speciated and total emission factors of  
801 particulate organics from burning western U.S. wildland fuels and their dependence on  
802 combustion efficiency, *Atmospheric Chemistry and Physics Discussions*, 1-22, 2018.

803 Kaur, R., and Anastasio, C.: Light absorption and the photoformation of hydroxyl radical and  
804 singlet oxygen in fog waters, *Atmos. Environ.*, 164, 387-397, 2017.

805 Kaur, R., and Anastasio, C.: First Measurements of Organic Triplet Excited States in  
806 Atmospheric Waters, *Environ. Sci. Technol.*, 52, 5218-5226, 2018.

807 Kozmér, Z., Arany, E., Alapi, T., Takács, E., Wojnárovits, L., and Dombi, A.: Determination of  
808 the rate constant of hydroperoxyl radical reaction with phenol, *Radiat. Phys. Chem.*, 102,  
809 135-138, 2014.

810 Lauraguais, A., Coeur-Tourneur, C., Cassez, A., and Seydi, A.: Rate constant and secondary  
811 organic aerosol yields for the gas-phase reaction of hydroxyl radicals with syringol (2, 6-  
812 dimethoxyphenol), *Atmos. Environ.*, 55, 43-48, 2012.

813 Lilie, J.: Pulsradiolytische untersuchung der oxydativen ringöffnung von furan, thiophen und  
814 pyrrol/pulsradiolytic investigations of the oxydativ ring scission of furan, thiophen and  
815 pyrrol, Zeitschrift für Naturforschung B, 26, 197-202, 1971.

816 McGregor, K. G., and Anastasio, C.: Chemistry of fog waters in California's Central Valley: 2.  
817 Photochemical transformations of amino acids and alkyl amines, Atmos. Environ., 35,  
818 1091-1104, 2001.

819 Meylan, W. M., and Howard, P. H.: Computer estimation of the atmospheric gas-phase reaction  
820 rate of organic compounds with hydroxyl radicals and ozone, Chemosphere, 26, 2293-  
821 2299, 1993.

822 Neta, P., and Schuler, R. H.: Rate constants for reaction of hydrogen atoms with aromatic and  
823 heterocyclic compounds. Electrophilic nature of hydrogen atoms, Journal of the  
824 American Chemical Society, 94, 1056-1059, 1972.

825 O'Neill, P., Steenken, S., and Schulte-Frohlinde, D.: Formation of radical cations of  
826 methoxylated benzenes by reaction with OH radicals, Ti<sup>2+</sup>, Ag<sup>2+</sup>, and SO<sub>4</sub><sup>•-</sup> in  
827 aqueous solution. An optical and conductometric pulse radiolysis and in situ radiolysis  
828 electron spin resonance study, Journal of Physical Chemistry, 79, 2773-2779, 1975.

829 O'Neill, P., and Steenken, S.: Pulse radiolysis and electron spin resonance studies on the  
830 formation of phenoxyl radicals by reaction of OH radicals with methoxylated phenols and  
831 hydroxybenzoic acids, Berichte der Bunsengesellschaft für physikalische Chemie, 81,  
832 550-556, 1977.

833 Parworth, C. L., Young, D. E., Kim, H., Zhang, X., Cappa, C. D., Collier, S., and Zhang, Q.:  
834 Wintertime water-soluble aerosol composition and particle water content in Fresno,  
835 California, J. Geophys. Res. Atmos., 122, 3155-3170, 2017.

836 Piechowski, M. V., Nauser, T., Hoignè, J., and Bühler, R. E.: O<sub>2</sub><sup>-</sup> decay catalyzed by Cu<sup>2+</sup> and  
837 Cu<sup>+</sup> ions in aqueous solutions: a pulse radiolysis study for atmospheric chemistry,  
838 Berichte der Bunsengesellschaft für physikalische Chemie, 97, 762-771, 1993.

839 Rehorek, D., and Seidel, A.: A. Leifer. The kinetics of environmental aquatic photochemistry.  
840 ACS professional and reference book. American Chemical Society, Washington 1988,  
841 304 S., 41 Abb., 35 Tab., Kart, Preis: US & Canada \$59.95, Export \$71.95, ISBN 0-  
842 8412-1464-6, Cryst. Res. Technol., 24, 732-732, 1989.

843 Richards-Henderson, N. K., Hansel, A. K., Valsaraj, K. T., and Anastasio, C.: Aqueous oxidation  
844 of green leaf volatiles by hydroxyl radical as a source of SOA: Kinetics and SOA yields,  
845 Atmos. Environ., 95, 105-112, 2014a.

846 Richards-Henderson, N. K., Pham, A. T., Kirk, B. B., and Anastasio, C.: Secondary Organic  
847 Aerosol from Aqueous Reactions of Green Leaf Volatiles with Organic Triplet Excited  
848 States and Singlet Molecular Oxygen, Environmental Science & Technology, 49, 268-  
849 276, 2014b.

850 Richards-Henderson, N. K., Pham, A. T., Kirk, B. B., and Anastasio, C.: Secondary organic  
851 aerosol from aqueous reactions of green leaf volatiles with organic triplet excited states  
852 and singlet molecular oxygen, Environ. Sci. Technol., 49, 268-276, 2014c.

853 Rinke, M., and Zetzsch, C.: Rate Constants for the Reactions of OH Radicals with Aromatics:  
854 Benzene, Phenol, Aniline, and 1, 2, 4-Trichlorobenzene, Ber. Bunsenges. Phys. Chem.,  
855 88, 55-62, 1984.

856 Rosario-Ortiz, F. L., and Canonica, S.: Probe compounds to assess the photochemical activity of  
857 dissolved organic matter, Environ. Sci. Technol., 50, 12532-12547, 2016.

858 Seinfeld, J. H., and Pandis, S. N.: Atmospheric chemistry and physics: From air pollution to  
859 climate change, John Wiley & Sons, 2012.

860 Smith, J. D., Sio, V., Yu, L., Zhang, Q., and Anastasio, C.: Secondary organic aerosol production  
861 from aqueous reactions of atmospheric phenols with an organic triplet excited state,  
862 Environ. Sci. Technol., 48, 1049-1057, 2014.

863 Smith, J. D., Kinney, H., and Anastasio, C.: Aqueous benzene-diols react with an organic triplet  
864 excited state and hydroxyl radical to form secondary organic aerosol, Phys. Chem. Chem.  
865 Phys., 17, 10227-10237, 2015.

866 Solar, S., Solar, W., and Getoff, N.: Reactivity of hydroxyl with tyrosine in aqueous solution  
867 studied by pulse radiolysis, J. Phys. Chem., 88, 2091-2095, 1984.

868 Tetreau, C., Lavalette, D., Land, E., and Peradejordi, F.: Sensitized triplet-triplet absorption of  
869 biphenylene, Chem. Phys. Lett., 17, 245-247, 1972.

870 Tratnyek, P. G., and Hoigne, J.: Oxidation of substituted phenols in the environment: a QSAR  
871 analysis of rate constants for reaction with singlet oxygen, Environmental science &  
872 technology, 25, 1596-1604, 1991a.

873 Tratnyek, P. G., and Hoigne, J.: Oxidation of substituted phenols in the environment: A QSAR  
874 analysis of rate constants for reaction with singlet oxygen, Environ. Sci. Technol., 25,  
875 1596-1604, 1991b.

876 USEPA: Estimation Programs Interface Suite™ for Microsoft® Windows, v 4.11, United States  
877 Environmental Protection Agency, Washington, DC, USA, 2012.

878 USGS: U.S. Geological Survey. Water Properties - Dissolved Oxygen. Available at  
879 <https://water.usgs.gov/edu/dissolvedoxygen.html> [last accessed: January 23, 2018], 2018.

880 Vempati, H. S.: Physico-chemical properties of green leaf volatiles, 2014.

881 Vione, D., Minella, M., Maurino, V., and Minero, C.: Indirect photochemistry in sunlit surface  
882 waters: photoinduced production of reactive transient species, Chemistry-A European  
883 Journal, 20, 10590-10606, 2014.

884 Wilkinson, F., Helman, W. P., and Ross, A. B.: Quantum yields for the photosensitized  
885 formation of the lowest electronically excited singlet state of molecular oxygen in  
886 solution, J. Phys. Chem. Ref. Data, 22, 113-262, 1993.

887 Wilkinson, F., Helman, W. P., and Ross, A. B.: Rate constants for the decay and reactions of the  
888 lowest electronically excited singlet state of molecular oxygen in solution. An expanded  
889 and revised compilation, J. Phys. Chem. Ref. Data, 24, 663-677, 1995.

890 Yasuhisa, T., Hideki, H., and Muneyoshi, Y.: Superoxide radical scavenging activity of phenolic  
891 compounds, International journal of biochemistry, 25, 491-494, 1993.

892 Young, D. E., Kim, H., Parworth, C., Zhou, S., Zhang, X., Cappa, C. D., Seco, R., Kim, S., and  
893 Zhang, Q.: Influences of emission sources and meteorology on aerosol chemistry in a  
894 polluted urban environment: results from DISCOVER-AQ California, Atmos. Chem.  
895 Phys., 16, 5427-5451, 2016.

896 Zein, A. E., Coeur, C. c., Obeid, E., Lauraguais, A. l., and Fagniez, T.: Reaction kinetics of  
897 catechol (1, 2-benzenediol) and guaiacol (2-methoxyphenol) with ozone, The Journal of  
898 Physical Chemistry A, 119, 6759-6765, 2015.

899 Zeng, T., and Arnold, W. A.: Pesticide photolysis in prairie potholes: probing photosensitized  
900 processes, Environmental science & technology, 47, 6735-6745, 2012.

901 Zepp, R. G., Braun, A. M., Hoigne, J., and Leenheer, J. A.: Photoproduction of hydrated  
902 electrons from natural organic solutes in aquatic environments, Environmental science &  
903 technology, 21, 485-490, 1987.

904 Zhou, X., and Mopper, K.: Determination of photochemically produced hydroxyl radicals in  
905 seawater and freshwater, Mar. Chem., 30, 71-88, 1990.

